https://doi.org/10.35662/unine-thesis-3209

Université de Neuchâtel
Faculté des Sciences
Institut de mathématiques

Thèse
présentée à la Faculté des Sciences pour l'obtention
du grade de docteur ès Sciences en mathématiques.

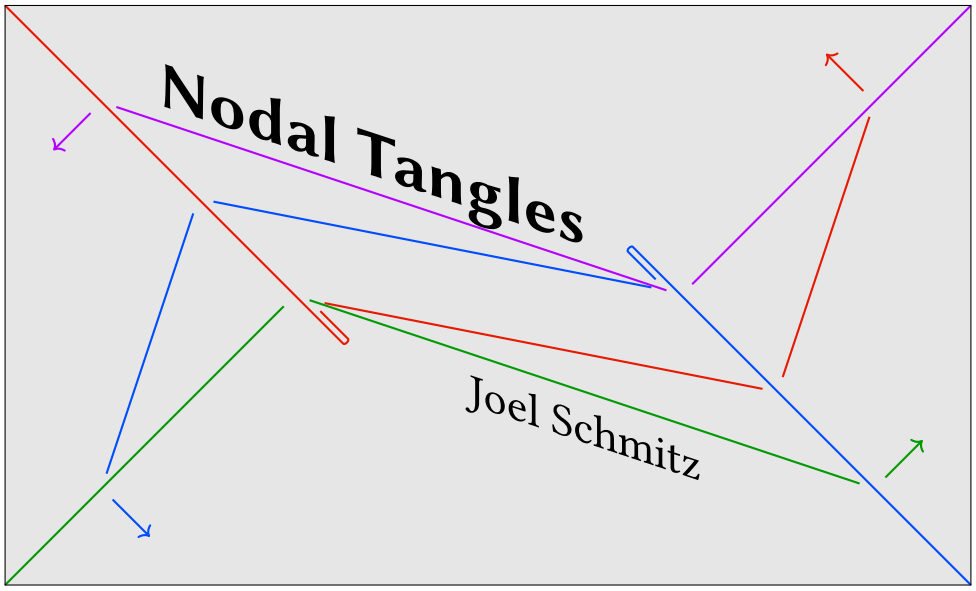

Acceptée sur proposition du jury :

Joé Brendel	ETH Zürich	directeur de thèse, rapporteur
Jonny Evans	Lancaster University	rapporteur
Peter Feller	Université de Neuchâtel	expert interne
Felix Schlenk	Université de Neuchâtel	directeur de thèse, rapporteur

Soutenue le 18 septembre 2025

unine
Université de Neuchâtel
Faculté des sciences

Rue Emile-Argand 11
CH-2000 Neuchâtel
doctorat.sciences@unine.ch

IMPRIMATUR POUR THESE DE DOCTORAT

La Faculté des sciences de l'Université de Neuchâtel autorise l'impression de la présente thèse soutenue par

Monsieur Joel SCHMITZ

Titre :

"Nodal Tangles"

sur le rapport des membres du jury composé comme suit :

- **Prof. Felix Schlenk,** directeur de thèse, Université de Neuchâtel, Suisse
- **Dr Joé Brendel,** co-directeur de thèse, ETHZ, Suisse
- **Prof. Peter Feller,** Université de Neuchâtel, Suisse
- **Prof. Jonathan David Evans,** University of Lancaster, UK

Neuchâtel, le 1er octobre 2025

Le Doyen, Prof. P. Brunner

Ein grosser Troubador,
man sucht seinesgleichen.
Solch einer kommt selten vor,
mindere müssen ihm weichen.

Zieht von Tür zu Tür,
reist von Tor zu Tor.
Wo immer seine Stimme klingt,
schenkt ein jeder ihm ein Ohr.

Findet fantast'sche Flöte.
Direkt in die Seel'
spielt sie ihm
manch' melodisches Juwel.

Aber ach! Die Welt
sie kann's nicht hören,
vernimmt nichts als
krächzen, kratzen, röhren.

Er kommt ihr abhanden;
sie lässt ihn zurück.
Er dichtet weiter
am nächsten Stück.

Steigt in künstlerische Höhen
spielt es allein dem Wind;
setzt's auf dessen Böen,
dass es in Zukunft jemand find'.

«Die Welt hat die Musik verloren,
Mit der ich sie einst erfüllt.
Mir ist als hätt' keine Ohren,
Hat sich der Schönheit verhüllt.

Ich bin gestorben dem Weltgewimmel
Und ruh' in einem stillen Gebiet.
Ich leb' in mir und meinem Himmel,
In meinem Lieben, in meinem Lied.»

Tommy Ash & Fredi Rückert

Résumé

Nous étudions les diagrammes de nœuds linéaires par morceaux dans la base des fibrations presque toriques des variétés symplectiques de dimension quatre. Ces diagrammes expriment des déformations de la fibration presque torique. Nous donnons plusieurs applications à la topologie symplectique, parmi lesquelles une preuve d'une conjecture de Symington, des contre-exemples plus simples à la récurrence de Poincaré lagrangienne en dimension quatre, le calcul de l'énergie de déplacement pour de nombreuses fibres de cartes de moment torique, et une recette élémentaire pour construire et distinguer des nœuds toriques lagrangiens.

Abstract

We study piecewise linear knot diagrams in the base of almost toric fibrations of symplectic four-manifolds. These diagrams translate to deformations of the almost toric fibration. We give several applications to symplectic topology, among them a proof of a conjecture by Symington, simpler counterexamples to Lagrangian Poincaré recurrence in dimension four, the calculation of the displacement energy for many fibres of toric moment maps, and an elementary recipe for building and distinguishing Lagrangian torus knots.

Mots-clés : géométrie symplectique, fibrations lagrangienne, applications moment, nœuds lagrangiens, récurrence de Poincaré lagrangienne.

Keywords: Symplectic Geometry, Lagrangian fibrations, moment maps, Lagrangian knots, Lagrangian Poincaré recurrence.

Acknowledgements

I would like to thank everyone who worked at the Institut de mathématiques[1] during my time here. You make it truly pleasant to come to university. Insbesondere Felix, Johannes und Joé möchte ich danken für all die fantastischen mathematischen und nichtmathematischen Diskussionen, dafür das ihr meinen halb garen Träumen gehör schenkt und mir helft die fehlenden Zutaten zu finden diese in die mathematische realität zu bringen. Merci aux étudiants de l'université pour m'apprendre le français et de me rappeler des difficultés des mathématiques élémentaires.

Danke an meine Familie, ohne eure Unterstützung wäre ich nicht bis zum Doktorat gekommen.

Thank you to all the wonderful associations providing me with extracurricular activities during my time in Neuchâtel. To Pange Lingua, Polyphonia and OG for letting me make music. Au Black Office pour m'apprendre dépanner mon vélo et ensuite me laissant partager ce savoir avec le monde. Grace à toi, ça rule.

And thank you to all my friends; whether we go on a hike, fix a bike, improve child safety, make music, hang out or take a forgetful group of adventurers to a damp swamp. Without you I wouldn't be myself.

[1] And Institut de biologie.

Contents

1 Introduction

Almost toric fibrations, that were introduced by Symington in [Sym03], have played a central role in symplectic topology over the last years. For instance, they have been used to construct Lagrangian torus knots [Via16; Via17; BHS24], to simplify known and establish new staircases for ellipsoid embeddings [CV22; Mag24; MS24], and to show that some rigidity results in algebraic geometry still persist in symplectic geometry [ES18]. When a symplectic 4-manifold (X, ω) admits an almost toric fibration, then many properties of (X, ω) can be read from the base B of the fibration, a two-dimensional integral affine surface with *nodes*. In this paper, we focus on how modifications of the nodal integral affine base B of the almost toric fibration translate to symplectic properties of the total space. Unlike the *mutations* used by Vianna in [Via16; Via17] for the same goal, where the shape of the base diagram changes, we will keep the shape of the base diagram fixed. This will improve or simplify some of the previous applications of almost toric fibrations and lead to new applications. A central concept of the paper are **nodal tangles** (Definition 2.20), which can be thought of as a sequence of *nodal slides* in the base B as defined in [Sym03], or equivalently as a certain smooth deformation of the nodal integral affine structure of B. In order to obtain applications of this combinatorial manipulation of B to symplectic geometry, we use three "translation theorems":

- Theorem 2.26 associates to a nodal integral affine surface a unique almost toric fibration.
- Theorem 2.29 describes how a nodal tangle gives rise to a path of almost toric fibrations.
- Corollary 2.34 describes how symplectic invariants of Lagrangian tori change along nodal tangles.

These three translation theorems are reformulations of results from [Sym03; Eva23; BHS24].

In Chapter 2 we define nodal integral affine surfaces and nodal tangles, give some tools which allow us to manipulate nodal integral affine surfaces, and formulate the three translation theorems above precisely.

In Chapter 3 we use the setup of Chapter 2 and results from elementary tropical geometry in [MS23] to show that a certain class of nodal integral affine surfaces, which includes Delzant polygons, can be deformed by a nodal tangle into a *canonical form*. We use this canonical form to prove three results, summarized in Sections 1.1 to 1.3.

In Chapter 4 we use nodal tangles to provide an elementary recipe for building

and distinguishing Lagrangian torus knots using nodal tangles, summarized in Section 1.4. The same combinatorics lead to an interesting example regarding Lagrangian pinwheels, connecting to the recent work [UZ25] describing which Wall singularities can arise in degenerations of del Pezzo surfaces, described in Section 1.5.

1.1 Symington's conjecture

Conjecture 6.8 in [Symo3] states that given two toric moment maps on a four dimensional symplectic manifold, we can always find a family of almost toric fibrations interpolating between them. We prove this conjecture for closed toric symplectic four-manifolds:

Theorem A (Corollary 3.26)**.** *Let $\mu_i : X \to \Delta_i$ with $i \in \{0,1\}$ be two toric moment maps on a closed four dimensional symplectic manifold. Then Δ_0 and Δ_1 are connected by a nodal tangle.*

In particular, there is a continuous path of almost toric fibrations $\pi_t : X \to B_t$ with $B_0 = \Delta_0$ and $B_1 = \Delta_1$.

A toric moment map on a symplectic manifold (X, ω) describes a strong set of symmetries (in the sense of Noether) of the space (X, ω). Theorem A says that any two such sets of symmetries must be related by a nodal tangle.

For the proof, we first deform both Δ_0 and Δ_1 by a nodal tangle into their canonical form, and then show that the canonical form only depends on the manifold X, which means that Δ_0 and Δ_1 have the same canonical form. The path of almost toric fibrations is then obtained using Theorem 2.29, the translation theorem allowing us to "lift" a nodal tangle to a one-parameter family of almost toric fibrations.

1.2 Lagrangian Poincaré non-recurrence

In [Sch24] we constructed a counterexample to Lagrangian Poincaré recurrence in dimension four using almost toric fibrations. That is, we constructed a Hamiltonian diffeomorphism ψ and a Lagrangian L such that $\psi^n(L) \cap L = \emptyset$ for all $n \in \mathbb{N}$ in a symplectic four manifold. Counterexamples in dimension six and higher had been found shortly before in [BS24]. See [Sch24] for a discussion of related results.

In Section 3.3 we use nodal tangles and the canonical form developed in Section 3.1 to put the construction of [Sch24] in a more general context and also provide a slightly different construction to give more counterexamples. Specifically, we construct counterexamples in all compact non-monotone toric symplectic four manifolds:

Theorem B. *For a compact non-monotone toric symplectic four manifold (X, ω), let $\pi : (X, \omega) \to B$ be the almost toric fibration over the canonical form B of X, and*

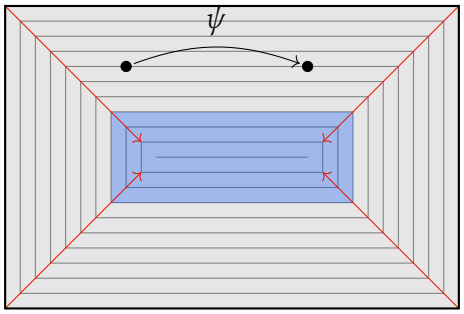

Figure 1.1: The behaviour of ψ on the base space $\square$ for $S^2 \times S^2$. Nodes are represented by arrowheads, the emerging lines are branch cuts. Level sets of $\mathscr{F}$ are in grey. The shaded region in the middle is $\mathscr{F}^{-1}((M-\varepsilon, M])$.

let $\mathscr{F} : B \to \mathbb{R}$ *be the* height function, *and* $M = \max \mathscr{F}$. *For any* $\varepsilon > 0$ *there exists a Hamiltonian diffeomorphism* ψ *such that for almost all*[1] *points* x *in the set* $\mathscr{F}^{-1}([0, M-\varepsilon])$ *the pair* $(\pi^{-1}(x), \psi)$ *provides a counterexample to Lagrangian Poincaré recurrence.*

The height function $\mathscr{F}$ measures the distance to the boundary B, such that $\mathscr{F}^{-1}([0, M-\varepsilon])$ is a set of measure arbitrarily close to the area of B. See also the following example.

Example 1.1. We quickly describe the effect of the constructed Hamiltonian diffeomorphism ψ in the case of non-monotone $S^2 \times S^2$, illustrated in Figure 1.1. Take $\omega_{a,b}$ to be the product symplectic form on $S^2 \times S^2$ giving areas $a > b$ to the factors. This admits a unique split toric moment map $\mu : S^2 \times S^2 \to \square$, where $\square \subset \mathbb{R}^2$ is an axis-aligned rectangle of side lengths a, b. After a nodal trade at each corner we have a base diagram as in Figure 1.1, giving a new fibration $\pi : S^2 \times S^2 \to \square$. The height function $\mathscr{F}$ gives the integral affine distance to the boundary of $\square$. Its level sets are also highlighted in Figure 1.1; its maximum is $M = \frac{b}{2}$. Let $\varepsilon > 0$. We can assume that all nodes are contained in the set $\mathscr{F}^{-1}((M-\varepsilon, M])$, highlighted in blue in Figure 1.1. Then the Hamiltonian diffeomorphism ψ is fibred with respect to π on the set $\mathscr{F}^{-1}([0, M-\varepsilon])$ and acts as follows on the fibres of π: Take $h \in [0, M-\varepsilon]$. Note that the integral affine structure on $\square$ induced by π (see Chapter 2) makes the level set $\mathscr{F}^{-1}(h)$ into a straight line. The Hamiltonian diffeomorphism ψ sends the fibre over a point $x \in \mathscr{F}^{-1}(h)$ to the fibre over the point x translated by a distance of $2(M-h)$ along $\mathscr{F}^{-1}(h)$ in the clockwise direction. The length of $\mathscr{F}^{-1}(h)$ is $a - b + 8(M-h)$, so if $\frac{M-h}{a-b}$ is irrational, then any fibre over a point $x \in \mathscr{F}^{-1}(h)$ and ψ give a counterexample to Lagrangian Poincaré recurrence.

Thus we can (partly) classify points $x \in \square$ depending on whether Lagrangian Poincaré recurrence holds for the fibre $\pi^{-1}(x)$:

[1] With respect to the Lebesgue measure on B.

- If $\frac{M-h}{a-b}$ is irrational, then Lagrangian Poincaré recurrence for fibres over $\mathscr{F}^{-1}(h)$ does not hold.
- If x is in the interior of the line segment $\mathscr{F}^{-1}(M)$, Lagrangian Poincaré recurrence does hold.
- If x is in a level set $\mathscr{F}^{-1}(h)$ with $\frac{M-h}{a-b}$ rational, or x is one of the end points of the line segment $\mathscr{F}^{-1}(M)$, it is unknown whether Lagrangian Poincaré recurrence holds.

The second point is proven in [PS24, Theorem C]. For convenience see also the reformulation [BK25, Theorem 1.15].

1.3 Displacement energy of toric fibres

Our third result in Chapter 3 concerns the displacement energy of fibres of toric moment maps. The displacement energy of a set $A \subset (X, \omega)$ is given by

$$e(A, X) := \inf\left\{\|H\| \;\middle|\; \begin{array}{l} H \text{ is a time-dependent compactly supported Hamiltonian} \\ \text{on } X \text{ such that its time-1 flow } \varphi_H^1 \text{ satisfies } \varphi_H^1(A) \cap A = \emptyset \end{array}\right\},$$

where

$$\|H\| = \int_0^1 \left(\sup_{x\in X}\{H_t(x)\} - \inf_{x\in X}\{H_t(x)\}\right)dt$$

is the Hofer norm. The displacement energy gives a symplectic invariant of the set A. In particular, it gives an invariant of Lagrangian tori.

The moment polygon Δ of a toric moment map $\mu : X \to \Delta$ is given by the intersection of half-planes

$$\langle \lambda_i, x\rangle + c_i \geq 0,$$

where $\lambda_i \in \mathbb{Z}^2$ are primitive vectors. Define

$$\mathscr{F}_\Delta : \Delta \to \mathbb{R}_{\geq 0}\,, \quad \mathscr{F}_\Delta(x) := \min\{\langle \lambda_i, x\rangle + c_i\}\,,$$

where we take the minimum over all the half-planes defining an edge of Δ. Hence $\partial\Delta = \mathscr{F}_\Delta^{-1}(0)$ and $\mathscr{F}_\Delta$ gives a notion of distance to the boundary of Δ.[2]

The canonical form constructed in Section 3.1 gives an almost toric fibration on X, and we can use probes in its nodal integral affine base to calculate the displacement energy for toric fibres:

Theorem C (Corollary 3.32)**.** *Let $\mu : X \to \Delta$ be a toric moment map on a symplectic four manifold. Except on a one-dimensional subset of Δ, called the* caustic*, if $\mathscr{F}_\Delta(x) < \frac{1}{2}\sup \mathscr{F}_\Delta$ the displacement energy of a fibre is given by*

$$e(\mu^{-1}(x)) = \mathscr{F}_\Delta(x)\,.$$

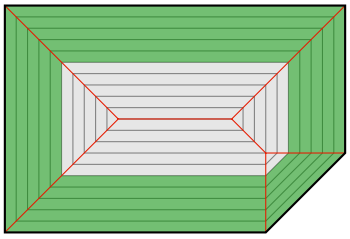

Figure 1.2: The green area marks the fibres displaceable via Theorem C, the red curve marks the caustic, the excluded one-dimensional subset.

See Figure 1.2 for an illustration.

The exclusion of the one-dimensional caustic in Theorem C is often irrelevant for distinguishing Lagrangian tori, as it often suffices to know e on an open dense subset of fibres of μ.

For any $x \in \Delta$, the lower bound $e(\mu^{-1}(x)) \geq \mathscr{F}_\Delta(x)$ is shown to always hold in [Bre23, Proposition 3.2]. The upper bound $e(\mu^{-1}(x)) \leq \mathscr{F}_\Delta(x)$ is not always known to hold. Outside the caustic, it can sometimes be proven in explicit examples using probes, see [McD11], or extended probes, see [ABM14], where we can use [Bre23, Proposition 3.4] to get the displacement energy.

Remark 1.2. If $\sup \mathscr{F}_\Delta = \infty$ in Theorem C, then every fibre outside the caustic is displaceable by a probe, providing an improvement on the method of extended probes used in [ABM14, Proposition 4.4.4]. For example all fibres in the white region in [ABM14, Figure 4.5.3] can be displaced by a probe using the canonical form as a base diagram.

Remark 1.3. For all examples of Delzant polygons I examined, the method of proof of Theorem C can be modified to give $e(\mu^{-1}(x)) = \mathscr{F}_\Delta(x)$ for all fibres outside the caustic, even without the condition $\mathscr{F}_\Delta(x) < \frac{1}{2} \sup \mathscr{F}_\Delta$, see Remark 3.33.

1.4 Lagrangian knots

The study of Lagrangian knots in a symplectic manifold (X, ω) involves classifying embedded Lagrangians in X up to either Lagrangian isotopy, symplectomorphism or Hamiltonian diffeomorphism, see [PS24] for a survey. In this paper we are concerned with the classification up to symplectomorphism. When constructing Lagrangian knots, we often want to rule out that two Lagrangians L_0, L_1 are not related by a symplectomorphism for "obvious" reasons, such as being topologically different or having different area classes $[\omega] : H_2(X, L_i) \to \mathbb{R}$. The following definition gives a criterion for when two Lagrangians are sufficiently similar that telling them apart becomes interesting.

[2] Sometimes $\mathscr{F}_\Delta$ is described as *integral affine distance to* $\partial\Delta$. Since the integral affine length (Definition 2.16) does not induce a metric, this is ambiguous.

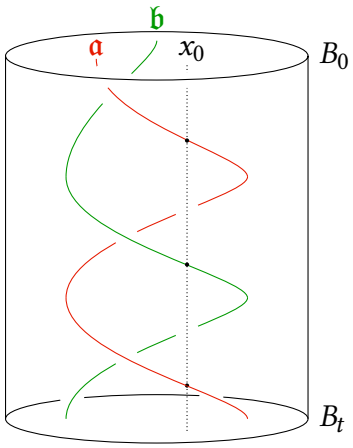

Figure 1.3: A topological picture of a nodal tangle used to produce Lagrangian knots. Here we slide two nodes $\mathfrak{a}, \mathfrak{b}$ alternatingly over x_0.

Definition 1.4. Two Lagrangian embeddings $\varphi_0, \varphi_1 : L \to X$ are **almost Hamiltonian isotopic** if for any neighbourhood U of $0 \in H^1(L; \mathbb{R})$ there is a Lagrangian isotopy $\varphi : L \times [0,1] \to X$ between them such that

$$\forall t \in [0,1], \quad \mathrm{Flux}(\varphi|_{L\times[0,t]}) \in U,$$

where Flux is the *Lagrangian flux map*.

The Lagrangian flux map is defined by measuring the symplectic area swept out by a representative of an element of $H_1(L)$ under the Lagrangian isotopy, see [BHS24, Definition 3.2] for details. If $\mathrm{Flux}(\varphi|_{L\times[0,t]}) = 0$ for all t, then the Lagrangian isotopy can be realized by an ambient Hamiltonian isotopy ([BHS24, Lemma 3.3]), and the Lagrangians $\varphi_0(L)$ and $\varphi_1(L)$ are Hamiltonian isotopic. For example Vianna's tori in [Via16; Via17] are all almost Hamiltonian isotopic.

In Chapter 4 we describe how nodal integral affine surfaces can be used to construct almost Hamiltonian isotopic Lagrangian torus knots: Almost toric fibrations have been used to construct knotted Lagrangian tori in [Via16; Via17; Bre23; Bre25; BHS24] as follows. This method is due to Vianna in [Via16]. Let $\pi_0 : X \to B_0$ be an almost toric fibration, let $x_0 \in B_0$ be a regular value and let $\mathfrak{a}_1, \ldots, \mathfrak{a}_n \in B_0$ be nodes whose eigenlines run through x_0. Sliding the nodes $\mathfrak{a}_1, \ldots, \mathfrak{a}_n$ back and forth over x_0 we get a nodal tangle $B_0 \times \mathbb{R}_{\geq 0}$, that is, a one-parameter family of nodal integral affine surfaces B_t with $t \geq 0$, and a corresponding family of almost toric fibrations $\pi_t : X \to B_t$, see Figure 1.3. By sliding the nodes $\mathfrak{a}_1, \ldots, \mathfrak{a}_n$ back and forth over x_0 we modify the integral affine structure of B_0 near x_0, as well as the fibration π_t. The fibre $\pi_0^{-1}(x_0)$ is a Lagrangian torus. By sliding a node over x_0, we modify the fibre $\pi_0^{-1}(x_0)$ by a *la-disc surgery* as in [STW16]. Almost toric fibrations now provide a convenient way to distinguish the modified fibres from the original ones: Let $\mathscr{L}$ denote the space of Lagrangians in X and let $\mathscr{I} : \mathscr{L} \to A$ be an invariant of

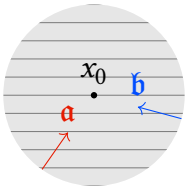

Figure 1.4: Two nodes $\mathfrak{a}, \mathfrak{b}$, marked by arrowheads, whose eigenlines pass through x_0. The eigenlines are parallel to the primitive integer vectors $v_\mathfrak{a}, v_\mathfrak{b}$ (the direction of the arrow tips). The level sets of the invariant $\mathscr{I}$ are in grey.

Lagrangians up to symplectomorphism with values in some set A. The germ $[\mathscr{I}]_{x_0}$ given by evaluating $\mathscr{I}$ on fibres near $x_0 \in B_0$ only depends on the fibre $\pi_0^{-1}(x)$ (Lemma 2.36). After having slid n nodes back and forth over x_0, the germ $[\mathscr{I}]_{x_0}$ is modified by the *transition map* τ_0^n, a piecewise affine map which describes how the integral affine structure changes near x_0 (Corollary 2.34). Then if $[\mathscr{I}]_{x_0}$ and $[\mathscr{I}]_{x_0} \circ \tau_0^n$ are not related by an integral linear transformation, the fibres $\pi_0^{-1}(x_0)$ and $\pi_n^{-1}(\tau_0^n(x_0))$ cannot be related by a symplectomorphism. So when we want to create Lagrangian knots, we can try to create "complicated" transition maps τ_0^n in order to change the invariant germ $[\mathscr{I}]_{x_0}$ enough to be distinguishable.

Using an invariant germ to distinguish Lagrangian tori has two advantages compared to using a holomorphic disc count as done in [Via16; Via17]: First, we can also treat non-monotone tori, that is, the point x_0 does not need to be the centre of a monotone moment polytope Δ, since the displacement energy germ can be calculated also for non-monotone tori, whereas it is difficult to calculate the holomorphic disc count of non-monotone Lagrangian tori. Second, the combinatorics of constructing the Lagrangian knot are directly linked to the invariant germ via the integral affine structure of the base. This allows us to construct and distinguish Lagrangian knots over many more points x in the base. See Example 4.7 and Section 5.4 for a discussion on how many families of knotted tori can be obtained using this method.

Theorem 4.6 describes a particular but still quite general situation in which we get infinitely many different Lagrangian tori over a point x_0, illustrated in Figure 1.4.

Theorem D (Theorem 4.6)**.** *Suppose that $\mathfrak{a}, \mathfrak{b}$ are two nodes of multiplicity $k_\mathfrak{a}, k_\mathfrak{b}$ with eigenlines running through x_0 in directions $v_\mathfrak{a}, v_\mathfrak{b}$, and that*

1. $k_\mathfrak{a} k_\mathfrak{b} \det(v_\mathfrak{a}, v_\mathfrak{b})^2 \geq 4$,
2. *The germ $[\mathscr{I}]_{x_0} : B_0 \dashrightarrow \mathbb{R}$ is affine and non-constant on an open dense set around x_0.*

Then the invariant germs $[\mathscr{I}]_{x_0} \circ \tau_n^0$ with $n \in \mathbb{Z}_{\geq 0}$ are pairwise different, hence the Lagrangian tori $\{\pi_n^{-1}(\tau_0^n(x_0))\}_n$ are pairwise not related by symplectomorphism.

Remark 1.5. The assumption that $[\mathscr{I}]_{x_0}$ is affine near x_0 is for example fulfilled for the displacement energy germ of all points in a Delzant polytope at which Theorem C holds.

Examples of infinite families of non-monotone tori have previously been constructed in [Bre25] in dimension six and in [BHS24] in dimension four, both also using the displacement energy germ as distinguishing invariant.

Remark 1.6. Another candidate for a good choice of $\mathscr{I}$ is the Ψ invariant described in [STV24]. In this paper the authors calculate Ψ for toric fibres of $\mu : X \to \Delta$, where X is a Fano variety of any dimension, in which case they find $\Psi(\mu^{-1}(x)) = \mathscr{F}_\Delta(x)$, where $\mathscr{F}_\Delta$ is defined analogously for the higher dimensional polytope Δ. Note however that X being Fano means that X is a monotone symplectic manifold; in particular if X is four dimensional, then X is a del Pezzo surface and the caustic of Δ is star shaped. Thus only the monotone fibre can have eigenlines of two nodes passing through its base point, and we are in the situation described in [Via17].

1.5 Lagrangian pinwheels

Another application of the above combinatorics used to construct Lagrangian knots is the construction of *Lagrangian pinwheels*. For coprime $p, q \in \mathbb{Z}$, the Lagrangian pinwheel $L_{p,q}$ is an embedded Lagrangian CW-complex which arises in algebraic geometry as the vanishing cycle of a $\mathbb{Q}$-Gorenstein smoothing of a Wahl singularity. Alternatively, they can be seen as *visible Lagrangians* lying over an eigenray of a node $\mathfrak{a}$ connecting it to ∂B. In the recent work [UZ25], the authors use methods from algebraic geometry to show which Wahl singularities can arise from degenerations of del Pezzo surfaces. In particular, [UZ25, Theorem 1.10] implies that any monotone symplectic $\mathbb{C}P^2 \# n\overline{\mathbb{C}P^2}$ with $5 \leq n \leq 8$ admits an embedding of $L_{p,q}$ for any coprime $p, q \in \mathbb{Z}$. In Example 4.9 we give an alternative construction of these pinwheels using our methods.

2 Nodal integral affine surfaces & almost toric fibrations

In Section 2.1 we define nodal integral affine surfaces independently from almost toric fibrations and setup some useful language to talk about them. In Section 2.2 we introduce nodal tangles and give a worked out examples how they can be manipulated. In Section 2.3 we relate nodal integral affine surfaces and nodal tangles to almost toric fibrations using [Symo3; Eva23], giving our first two translation theorems 2.26 and 2.29. In Section 2.4 we describe how invariant germs change under nodal tangles, giving our third translation theorem 2.34.

2.1 Nodal integral affine surfaces

Denote by $\mathrm{Aff}_n(\mathbb{Z}) = \mathrm{GL}_n(\mathbb{Z}) \rtimes \mathbb{R}^n$ the group of integral affine transformations of $\mathbb{R}^n$.

Definition 2.1. An **integral affine manifold** B is a smooth manifold with corners with an *integral affine structure*, that is an equivalence class of atlases $\{\varphi_i : B \supset U_i \to \mathbb{R}^n_{\geq 0}\}_{i\in I}$ such that the transition functions $\varphi_i \circ \varphi_j^{-1}$ are elements of $\mathrm{Aff}_n(\mathbb{Z})$.

The **integral lattice bundle** of B is the lattice bundle $\Lambda B \subset TB$ given by the pullback of $\mathbb{Z}^n \subset \mathbb{R}^n$ under integral affine charts. The **dual integral lattice bundle** $\Lambda^* B \subset T^*B$ is the lattice bundle dual to ΛB.

Definition 2.2. An **integral affine map** $\psi : A \to B$ between integral affine manifolds is a map such that for all integral affine charts φ_A, φ_B on A, B respectively, $\varphi_B \circ \psi \circ \varphi_A^{-1} \in \mathrm{Aff}_n(\mathbb{Z})$.

A **piecewise integral affine**[1] **map** $\tau : A \to B$ is a continuous map such that there exists a triangulation of A by a polyhedral complex Δ such for any cell σ of Δ, the restriction $\tau|_\sigma$ is integral affine.

Definition 2.3. A **piecewise integral linear map** $R : \mathbb{R}^n \to \mathbb{R}^m$ of is a continuous map such that there exists a fan[2] Δ on $\mathbb{R}^n$ such that for any cone c of Δ the restriction $R|_c$ is an element of $\mathrm{GL}_n(\mathbb{Z})$.

[1] We want to distinguish piecewise affine and piecewise *linear* maps (defined below), so here we use the non-standard but more sensible "affine".

[2] i.e. a polyhedral complex where every cell is a cone.

Definition 2.4. The **cut complex** of a piecewise integral affine map $\tau : A \to B$ is the minimal polyhedral complex Δ on A such that for every cell c the restriction $\tau|_c$ is integral affine.

Definition 2.5. A **pre-nodal integral affine manifold** of dimension n is a pair $(B, \mathfrak{N})$ where

- B is a smooth n-dimensional manifold with corners,
- $\mathfrak{N} \subset B$ is a closed stratified subspace with top dimension $n-2$,
- $B \setminus \mathfrak{N}$ is an integral affine manifold with corners.

The points of the set $\mathfrak{N}$ are called **nodes**.

We will be mostly interested in the case $n = 2$, where $\mathfrak{N}$ is a closed set of isolated points in B. The case $n = 3$ will be relevant for Definition 2.20, where we will be mostly interested in the case where $\mathfrak{N}$ is a closed 1-dimensional embedded submanifold.

Let $(B, \mathfrak{N})$ be a pre-nodal integral affine surface. An integral affine chart on $B \setminus \mathfrak{N}$ cannot describe the neighbourhood of a node. The following definition tries to address this drawback. The concept is similar to that of a base diagram used e.g. in [Sym03; Eva23].

Definition 2.6. Let $U \subset B$ be open. A **nodal chart** on U is a homeomorphism onto its image $\varphi : U \to \mathbb{R}^2$ that is piecewise integral affine on $U \setminus \mathfrak{N}$.

Definition 2.7. For any nodal chart $\varphi : U \to \mathbb{R}^2$ and any point $x \in U \setminus \mathfrak{N}$, after a translation taking $\varphi(x)$ to 0, there is an invertible piecewise integral linear map $R_x : \mathbb{R}^2 \to \mathbb{R}^2$ such that $R_x \circ \varphi$ is an integral affine chart on a neighbourhood of x. We call R_x the **rectifying map of φ at x**.

The rectifying map is unique up to composing with an integral linear map. For x in the integral affine locus of φ, we may choose $R_x = \mathrm{id}$.

The 1-cells of the cut complex of φ^{-1} form an embedded graph G in $\operatorname{im}\varphi$. The edges of G have rational slope (see Remark 2.8 below). We call G the **cut graph of φ^{-1}** and the edges of G **cuts of φ^{-1}**.[3]

Remark 2.8. Suppose $x \in B \setminus \mathfrak{N}$ is a point such that $\varphi(x)$ is in the interior of a cut ℓ, as in Figure 2.1. Then its rectifying map R_x is given by two integral affine maps that agree on ℓ. W.l.o.g. we may take one of them to be the identity. Then the other one must fix ℓ, and thus is the integral shear map $s_v^k(y) = y - kv\det(v, y)$, where v is a primitive vector along ℓ, and k a positive integer. Requiring k to be positive induces an orientation on ℓ, given by v. So R_x must be equal to the **half-shear**

$$h_v^k(y) = \begin{cases} s_v^k(y) & \text{if } \det(v, y) \geq 0 \\ y & \text{if } \det(v, y) \leq 0 \end{cases}. \tag{2.1}$$

[3]The name comes from the similarity to *branch cuts* of almost toric base diagrams ([Eva23, Definition 8.3]). Since we're not cutting branches to get a fundamental domain of $B \setminus \mathfrak{N}$ in its universal cover, we just call them cuts, as we're still cutting the integral affine structure.

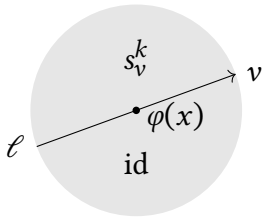

Figure 2.1: The rectifying map in the case of Remark 2.8.

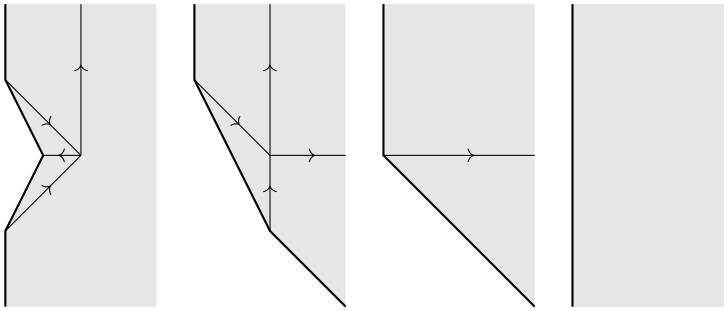

Figure 2.2: Four different nodal charts of $\mathbb{R}_{\geq 0} \times \mathbb{R}$. Each adjacent pair is related by a half-shear. On the right is the integral affine chart $\mathrm{id}_{\mathbb{R}_{\geq 0}\times\mathbb{R}}$.

This makes G into a directed weighted graph, with direction on ℓ given by v and weight given by k. The pair $(\operatorname{im}\varphi, G)$ lets one reconstruct the integral affine structure on $U \setminus \mathfrak{N}$. See Figure 2.2 for an example. We call the pair $(\operatorname{im}\varphi, G)$ a **nodal chart diagram**.

Definition 2.9. A nodal chart $\varphi : U \to \mathbb{R}^2$ is called **simple** if all vertices of the cut graph G are 1-valent, i.e. G is a disjoint union of line segments.

Definition 2.10. A **nodal integral affine surface** is a pre-nodal integral affine surface $(B, \mathfrak{N})$ such that every node $\mathfrak{a} \in \mathfrak{N}$ admits a simple nodal chart $\varphi : U_{\mathfrak{a}} \to \mathbb{R}^2$ such that $\varphi(\mathfrak{a})$ is a vertex of the cut graph of φ^{-1} and the edge adjacent to $\varphi(\mathfrak{a})$ is an incoming edge, see Figure 2.3.

The weight of the incoming edge at $\varphi(\mathfrak{a})$ is called the **multiplicity** of $\mathfrak{a}$.

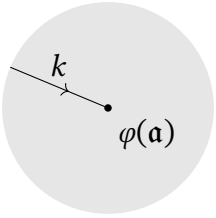

Figure 2.3: A nodal chart diagram of a neighbourhood of a node $\mathfrak{a}$ of multiplicity k.

The requirement that a node $\mathfrak{a}$ admits a simple nodal chart as in Definition 2.10 is equivalent to a node admitting a model neighbourhood as in [Sym03, Proposition 4.14], meaning that Definition 2.10 is equivalent to [Sym03, Definition 5.1].

Remark 2.11. One could be tempted to include "anti-nodes" in Definition 2.10, that is nodes with an outgoing edge of G at $\varphi(\mathfrak{a})$. These anti-nodes do not seem to have a corresponding concept in symplectic geometry or algebraic geometry (e.g. we would have to rule them out in Theorems 2.26 and 2.29), so we already rule them out in the definition.

We may think of the nodes as discrete points of positive curvature in the otherwise flat B. We have the following "affine Gauss-Bonnet theorem":

Theorem 2.12 ([KS06, Theorem 2])**.** *If B is compact and without boundary,*

$$\frac{1}{12}\sum_{\mathfrak{n}\in\mathfrak{N}} k_{\mathfrak{n}} = \chi(B)$$

where $k_{\mathfrak{n}}$ is the multiplicity of $\mathfrak{n}$, and χ denotes the Euler characteristic.

Remark 2.13. This leads to a very limited topology on nodal integral affine surfaces: If B is compact (perhaps with boundary/corners) then B is either a disc, an annulus, a Möbius band, a Klein bottle with no nodes, a torus with no nodes, a projective plane with 12 nodes or a sphere with 24 nodes. See [Zun03, Proposition 3.3]. [LS10] determines the corresponding symplectic manifolds up to diffeomorphism.

Given a topological covering $p : E \to X$, for a chosen base point $x \in X$ we get the *monodromy action* $\pi_1(X, x) \to \mathrm{Aut}(p^{-1}(x))$ obtained by lifting loops based at x to E. We are interested in the monodromy of the lattice bundle $\Lambda B \to (B \setminus \mathfrak{N})$ around a node.

Take a simple nodal chart $\varphi : U_{\mathfrak{a}} \to \mathbb{R}^2$ at $\mathfrak{a} \in \mathfrak{N}$ with the cut graph G of φ^{-1} and equip $U_{\mathfrak{a}}$ with the orientation induced by $\mathbb{R}^2$. Let ℓ be the incoming edge of G at $\mathfrak{a}$, $v' \in \mathbb{Z}^2$ its primitive direction vector of ℓ and k the weight of ℓ. Then the monodromy of ΛB induced by a positive loop around $\mathfrak{a}$ based at $x \in U_{\mathfrak{a}} \setminus \{\mathfrak{a}\}$ is given by the shear map $(D_x\varphi)^{-1} \circ s_{v'}^k \circ D_x\varphi$. Here $D\varphi_x$ is defined if x does not lie on a cut of φ. As v' is fixed by the monodromy, the pull-back $v = D\varphi^{-1}[v']$ gives a well-defined vector field on $U_{\mathfrak{a}}$, that is there is a unique continuous vector field v such that $D\varphi[v] = v'$ whenever $D\varphi$ is defined. Similarly $\lambda = \varphi^*(\det(v', \cdot))$ gives a well-defined covector field on $U_{\mathfrak{a}}$. We can thus write the monodromy of a positive loop around $\mathfrak{a} \in B$ as

$$\mathrm{id} - k v\lambda\ .$$

The monodromy is independent of the choice of simple nodal chart, so the pair (v, λ) is unique up to sign. We call the pair (v, λ) the **monodromy pair of $\mathfrak{a}$**, v the **monodromy vector field** and λ the **monodromy covector field**.[4]

[4]Note that here λ has only an auxiliary function: If we choose an orientation around $\mathfrak{a}$, it is given by $\det(v, \cdot)$.

The integral lattice ΛB also induces a connection on $TB \to (B \setminus \mathfrak{N})$: By lifting paths in $B \setminus \mathfrak{N}$ to ΛB, we get a parallel transport system on $\Lambda B \to B \setminus \mathfrak{N}$, which can be linearly extended to $TB \to B \setminus \mathfrak{N}$. A geodesic with respect to this connection is a path γ such that $\dot{\gamma}$ is constant relative to ΛB, which motivates the following definition:

Definition 2.14. A **straight line** γ in $B \setminus \mathfrak{N}$ is a geodesic with respect to the connection induced by the integral lattice ΛB.

- We say γ is **maximal** if it cannot be extended in $B \setminus \mathfrak{N}$.
- It is **rational** if $r\dot{\gamma} \in \Lambda B$ for some real number $r > 0$.
- It is **primitive** if $\dot{\gamma} \in \Lambda B$ is primitive.

Remark 2.15. A straight line might have self-intersections.

We think of primitive straight lines as having "unit speed":

Definition 2.16. Let $\gamma : (a, b) \to B \setminus \mathfrak{N}$ be a rational straight line with $r\dot{\gamma} \in \Lambda B$ primitive. Its **integral affine length** is given by $\frac{b-a}{r}$.

Note that this notion of length does not induce a well-defined metric.

Definition 2.17. Let $\mathfrak{a} \in \mathfrak{N}$. The **eigenline** γ **of** $\mathfrak{a}$ is the one-dimensional subset of B with $\mathfrak{a} \in \gamma$ such that $\gamma \setminus \{\mathfrak{a}\}$ is the union of the two maximal straight lines which are parallel to the monodromy vector field of $\mathfrak{a}$ and whose closure includes $\mathfrak{a}$.

Remark 2.18. The eigenline of a node might be a circle, in which case the two maximal straight lines in the definition above coincide.

We will often want to know how images of straight lines in B look like in a nodal chart diagram. The following remark is a useful tool for this:

Remark 2.19. Take a nodal chart $\varphi : B \supset U \to \mathbb{R}^2$ and let $\gamma : (-\varepsilon, \varepsilon) \to B \setminus \mathfrak{N}$ be a straight line segment with $\gamma(0) = x \in U$. Then $\varphi \circ \gamma$ is a piecewise affine path, and $R_x \circ \varphi \circ \gamma$ is an affine path. Denote by $(\varphi \circ \gamma)'(0^{\pm})$ the upper resp. lower derivative of $\varphi \circ \gamma$ at 0. Then we have

$$R_x((\varphi \circ \gamma)'(0^+)) = -R_x(-(\varphi \circ \gamma)'(0^-)) ,$$

since R_x maps the vectors $\pm(\varphi \circ \gamma)'(0^{\pm})$ to $\pm(R_x \circ \varphi \circ \gamma)'(0)$.

Together with Remark 2.8, this translates to the following recipe: Let ℓ be a cut with primitive direction vector v. Approaching ℓ walking on a straight line in direction u, after going through ℓ we will exit on the other side of ℓ with direction $u + |\det(v, u)|v$.

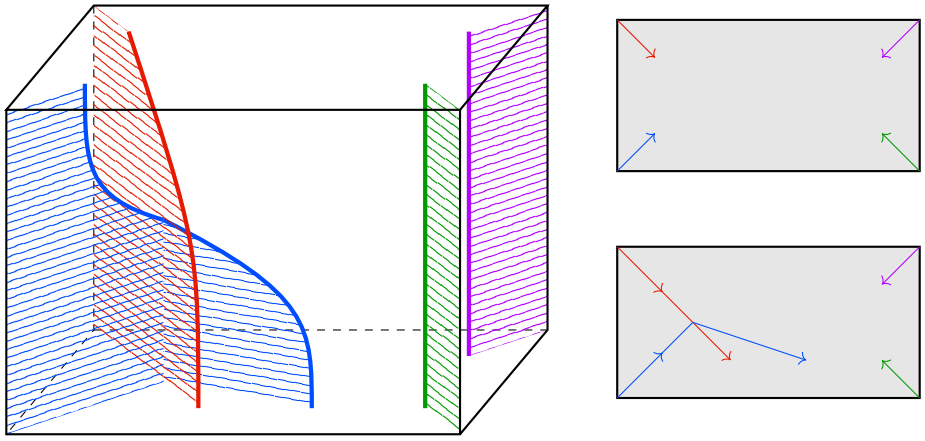

Figure 2.4: A nodal tangle. Horizontal slices are nodal chart diagrams. On the right are the top and bottom nodal chart diagrams. In the image on the left, the nodes $\mathfrak{N}$ are given by the thick coloured curves.

2.2 Nodal tangles

A nodal slide as in [Symo3, §6.1] can be described as two nodal integral affine surfaces that are identical except for one node which has been displaced along its eigenline. The following definition captures a notion of isotopy between two nodal integral affine surfaces constructed by a sequence of nodal slides.

Definition 2.20. A **nodal tangle** is a pre-nodal integral affine manifold $(B \times I, \mathfrak{N})$, where B is a surface with corners and I is an interval with its integral affine structure inherited from $\mathbb{R}$, such that:

- $B \setminus \pi_B(\mathfrak{N})$ is an integral affine surface such that $(B \setminus \pi_B(\mathfrak{N})) \times I$ is an integral affine submanifold of $B \times I \setminus \mathfrak{N}$.
- For every $t \in I$, $(B_t, \mathfrak{N}_t) = (B \times \{t\}, \mathfrak{N} \cap B \times \{t\})$ is a nodal integral affine surface which intersects $\mathfrak{N}$ transversely.
- For $t \in I$ and $\mathfrak{a} \in \mathfrak{N}_t$, let λ be the monodromy covector field of $\mathfrak{a} \in (B_t, \mathfrak{N}_t)$. Then for any 1-dimensional stratum S of $\mathfrak{N}$ at $(\mathfrak{a}, t)$ we have $D\pi_B(T_{(\mathfrak{a},t)}S) \subset \ker \lambda$.

Here $\pi_B : B \times I \to B$ denotes the projection to B.

We can think of a nodal tangle as a movie in which nodes can slide along their eigenlines, and a node of multiplicity k can split into multiple nodes with the same monodromy pair whose multiplicities add up to k. The first two conditions ensure that the integral affine structure on $B \setminus \pi_B(\mathfrak{N})$ remains fixed and that $\mathfrak{N}$ is not tangent to any B_t. The third condition ensures that nodes slide along their eigenline, as $\ker \lambda$ is spanned by the monodromy vector field v.

Definition 2.21. If $(B \times [a, b], \mathfrak{N})$ is a nodal tangle we say $(B_a, \mathfrak{N}_a)$ and $(B_b, \mathfrak{N}_b)$ are **connected by a nodal tangle**.

The following lemma states that this definition is compatible with [Symo3, §6.1]:

Lemma 2.22. *Two integral affine surfaces $(A, \mathfrak{N}_A), (C, \mathfrak{N}_C)$ are related by a finite sequence of nodal slides (see [Symo3, Definition 6.1/Exercise 6.7]) if and only if they are connected by a nodal tangle.*

Proof. Given $(A, \mathfrak{N}_A), (C, \mathfrak{N}_C)$ related by a single nodal slide we can easily construct a nodal tangle between $(A, \mathfrak{N}_A)$ and $(C, \mathfrak{N}_C)$. For a sequence of nodal slides we can stack the nodal tangles thus obtained on top of each other.

Given a nodal tangle $(B \times I, \mathfrak{N})$, for a subinterval $J \subset I$ let $(B \times J, \mathfrak{N}_J = \mathfrak{N} \cap B \times J)$ be the nodal tangle restricted to J. Restricting to a small enough subinterval $J = [a, b] \subset I$ the set $\pi_B(\mathfrak{N}_J)$ is a disjoint union of closed straight line segments in B, one for every connected component of $\mathfrak{N}_J$.

For connected components of $\mathfrak{N}_J$ which have no stratification (no nodes splitting), [Symo3, Definition 6.1] now gives a suitable nodal slide. For stratified components of $\mathfrak{N}_J$, we extend the definition of nodal slide [Symo3, Definition 6.1] to the case mentioned in [Symo3, Exercise 6.7].

Any order of these nodal slides gives a sequence of nodal slides transforming B_a into B_b.

Since I is compact by Definition 2.21, we only need finitely many subintervals J to cover I. □

Definition 2.23. Let $(B \times I, \mathfrak{N})$ be a nodal tangle, and let $a, b \in I$. The map $\tau_a^b : B_a \to B_b$ given by the composition $i_b \circ \pi_B$, where i_b is the natural homeomorphism $B \to B \times \{b\} = B_b$, is called **transition map**.

$\tau_a^b|_{B_a \setminus (\mathfrak{N}_a \cup \tau_b^a \mathfrak{N}_b)}$ is a piecewise integral affine map, with the restriction $\tau_a^b|_{B_a \setminus \pi_B \mathfrak{N}}$ being integral affine. It describes the changes in the integral affine structure induced by the nodal tangle. If φ_a is an integral affine chart near $x_a \in B_a$, then $\varphi_b = \varphi_a \circ \tau_b^a$ is a nodal chart near $x_b = \tau_a^b(x_a)$, whose cut graph G_b is contained in $\pi_B(\mathfrak{N})$ (although φ_b may still be an integral affine chart, in particular if $x_a \notin \pi_B(\mathfrak{N})$).

Example 2.24 (Building a nodal tangle)**.** Figure 2.5 a) shows a nodal chart diagram of a global simple nodal chart $\varphi_0 : (B_0, \mathfrak{N}_0) \to \mathbb{R}^2$, with four cuts ending in the nodes $\mathfrak{a}, \mathfrak{b}, \mathfrak{c}, \mathfrak{d}$ of multiplicity 1. The position of the nodes is marked by arrow tips. The direction of the arrow tips correspond to the orientation mentioned in Remark 2.8, and to the direction of the monodromy vector field of the node.

Let's modify $(B_0, \mathfrak{N}_0)$ by nodal slides to create a nodal tangle: First slide $\mathfrak{a}$ such that x is contained in its cut, giving the new nodal chart diagram for $\varphi_1 := \varphi_0 \circ \tau_1^0 : (B_1, \mathfrak{N}_1) \to \mathbb{R}^2$ as seen in Figure 2.5 b). In doing so we modified the integral affine structure along $\mathfrak{a}$'s cut. The rectifying map at the marked point x of φ_1 is now no longer trivial since x sits on a cut. Concretely, let $v_1 = \left(\begin{smallmatrix} 1 \\ -1 \end{smallmatrix}\right)$ be the direction of $\mathfrak{a}$'s cut, then R_x is the half-shear h_{v_1}, defined in (2.1).

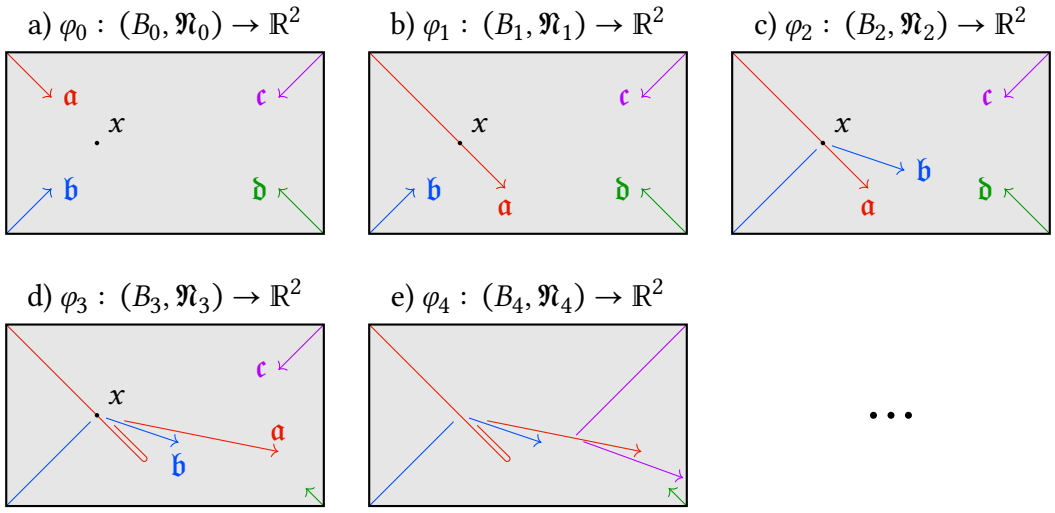

Figure 2.5: Building a tangle.

Moving on, we can slide $\mathfrak{b}$ along its eigendirection, past the point x. As our nodal chart φ_1 has a cut through x, the straight line segment in B along which we slide $\mathfrak{b}$ appears broken in $\operatorname{im}\varphi_1$ at the point x. Using the recipe in Remark 2.19, we find that the incoming vector $v_2' = \left(\begin{smallmatrix}1\\1\end{smallmatrix}\right)$ exits x as $v_2 = \left(\begin{smallmatrix}3\\-1\end{smallmatrix}\right)$:

$$v_2 = v_2' + |\det(v_1, v_2)|v_1 = \begin{pmatrix}1\\1\end{pmatrix} + 2\begin{pmatrix}1\\-1\end{pmatrix} = \begin{pmatrix}3\\-1\end{pmatrix}.$$

We get the nodal chart diagram Figure 2.5 c) for $\varphi_2 : (B_2, \mathfrak{N}_2) \to \mathbb{R}^2$. The rectifying map at x of φ_2 is now the composition $h_{v_2} \circ h_{v_1}$.

The tangle built up to this point is the one depicted in Figure 2.4, and we can obtain the diagram Figure 2.5 c) by projecting the left drawing in Figure 2.4 onto B. We indicate the order of the two nodal slides through x by drawing the later slide "underneath" the first, as in knot diagrams.

Sliding $\mathfrak{a}$ back through x, it is once again deflected, giving Figure 2.5 d). Using Remark 2.19 again, we determine the outgoing vector v_3 pointing from x to the node $\mathfrak{a}$ to be

$$v_3 = -v_1 + |\det(-v_1, v_2)|v_2 = \begin{pmatrix}-1\\1\end{pmatrix} + 2\begin{pmatrix}3\\-1\end{pmatrix} = \begin{pmatrix}5\\-1\end{pmatrix},$$

giving the new rectifying map $R_x = h_{v_3} \circ h_{v_2} \circ h_{v_1}$. Here the "hook" at x of $\mathfrak{a}$ going back along its path is technically not a cut of φ_3. However we still choose to draw it and think of the diagram as a projection of the nodal tangle $(B \times [0,3], \mathfrak{N})$.

Proceeding in the same manner we can continue to create more and more complicated nodal tangles.

Another example of a more complicated nodal tangle can be seen in Figure 2.6.

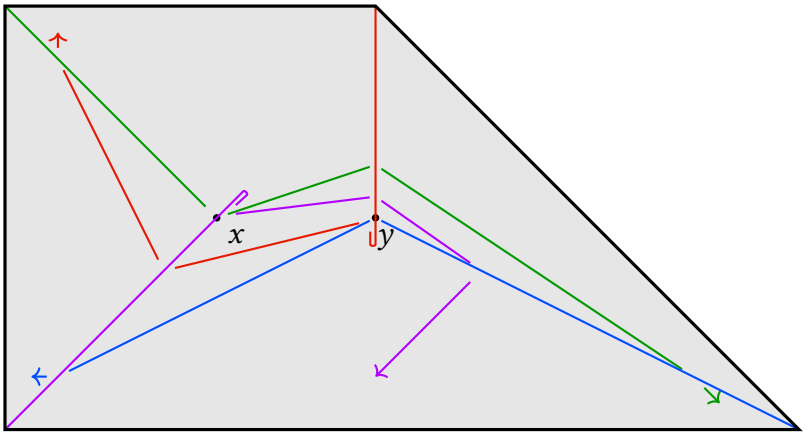

Figure 2.6: A more complicated tangle of nodes. The small hooks at x and y illustrate the node reversing its sliding direction, not an actual lateral movement.

Let $B \times [0,1]$ be a nodal tangle, and $\varphi_0 : B_0 \subset U_0 \to \mathbb{R}^2$ a simple nodal chart. Perturb $\mathfrak{N}$ (disregarding the integral affine structure) such that $\pi_B|_{\mathfrak{N}}$ is an immersion. The image of $\varphi_0 \circ \pi_B$ with over/under crossings of $\mathfrak{N}$ marked as in a knot diagram is called a **nodal tangle diagram**.

See for example the diagrams in Figures 2.5 and 2.6. The perturbation of $\mathfrak{N}$ creates the hooks. Due to the imprecision introduced by perturbing $\mathfrak{N}$, nodal tangle diagrams are mainly useful for illustration purposes. However, nodal tangle diagrams are still enough to reconstruct the nodal tangle $B \times I$ up to an appropriate notion of isotopy of nodal tangles.

2.3 Almost toric fibrations

Definition 2.25. Let (X, ω) be a 4-dimensional symplectic manifold, and B a smooth surface. An **almost toric fibration** is an integrable system $\pi : X \to B$ with compact connected fibres, non-degenerate singularities and no hyperbolic singularities.

See e.g. [Zuno3] for the definitions regarding integrable systems.

An almost toric fibration induces on B the structure of a nodal integral affine surface: Denote by $\mathfrak{N}$ the image of the focus-focus singularities of π. Then the Arnold-Liouville Theorem gives a set of charts on $B \setminus \mathfrak{N}$ called *action-coordinates*, with transition maps in $\mathrm{Aff}_2(\mathbb{Z})$. The pullback $\pi^* f$ of a local smooth function $f : B \supset U \to \mathbb{R}$ induces a Hamiltonian action on $\pi^{-1}(U)$. Similarly, any 1-form $\lambda \in T^*B$ is locally exact, and thus induces a local Hamiltonian action. We have $\lambda \in \Lambda^* B$ if and only if λ induces a local Hamiltonian S^1-action. The lattice $\Lambda^* B$ induces a local free Hamiltonian torus action near points of the **regular locus** $B \setminus (\partial B \cup \mathfrak{N})$.

The neighbourhood of a node $\mathfrak{n} \in \mathfrak{N}$ is described in [Zun97]; the existence of simple nodal charts is discussed in [Sym03, Section 4.4]. The fact that the monodromy covector field λ of a node $\mathfrak{n}$ extends over $\mathfrak{n}$ corresponds to the fact that $\pi^*\lambda$ induces an S^1 action on a neighbourhood of $\pi^{-1}(\mathfrak{n})$.

The fibre over a point $x \in B$ is a Lagrangian torus if x is a regular point, a circle if $x \in \partial B$ and not a corner, a point if x is a corner of B, and if x is a node of multiplicity k the fibre is a torus pinched k times along the monodromy covector field λ, that is we take k disjoint orbits of λ in a regular fibre nearby and collapse them to k points.

In certain cases a nodal integral affine surface uniquely determines an almost toric fibration:

Theorem 2.26. *Let $(B, \mathfrak{N})$ be an nodal integral affine surface. Then an almost toric fibration $\pi : X \to (B, \mathfrak{N})$ exists.*

If additionally B is homotopy equivalent to a punctured surface, the almost toric fibration is unique in the following sense: Suppose two almost toric fibrations $\pi_1 : X_1 \to B$ and $\pi_2 : X_2 \to B$ induce the same nodal integral affine structure on B. Then for any neighbourhood U of $\mathfrak{N}$ there exists a symplectomorphism $\psi : X_1 \to X_2$ such that

$$\begin{array}{ccc} X_1 \setminus \pi_1^{-1}(U) & \xrightarrow{\psi} & X_2 \setminus \pi_2^{-1}(U) \\ & {\scriptstyle \pi_1} \searrow \quad \swarrow {\scriptstyle \pi_2} & \\ & B & \end{array}$$

commutes, that is, except on a neighbourhood U of the nodes $\mathfrak{N}$, ψ is a fibred symplectomorphism*, .*

The existence is shown in [Sym03, Theorem 5.2], and uniqueness is shown in [Eva23, Proof of Theorem 8.5].

Remark 2.27. The ambiguity for the uniqueness comes only from the regular part $\widetilde{B} = B \setminus (\mathfrak{N} \cup \partial B)$, and is discussed in [Dui80, Section 2]. We summarize the discussion: The quotient $T^*\widetilde{B}/\Lambda^*\widetilde{B}$ carries a natural symplectic structure. Let $\mathscr{Z}(T^*\widetilde{B}/\Lambda^*\widetilde{B})$ denote the sheaf of Lagrangian sections $\widetilde{B} \to T^*\widetilde{B}/\Lambda^*\widetilde{B}$. Then for any element μ in the Čech cohomology $H^1(B, \mathscr{Z}(T^*\widetilde{B}/\Lambda^*\widetilde{B}))$, the data of $(B, \mathfrak{N}, \mu)$ determines a unique almost toric fibration in the sense of Theorem 2.26. See also [Zuno3] for putting this into the context of integrable systems with singularities.

Remark 2.28. [Sano3] describes the possible almost toric fibrations in the neighbourhood of a node up to fibred symplectomorphisms, which can be classified by a certain Taylor series. By allowing ψ to be not fibred near the nodes, we can ignore this subtlety.

A nodal tangle can be lifted to a path of almost toric fibrations:

Theorem 2.29. *Let $(B \times I, \mathfrak{N})$ be a nodal tangle, $a \in I$ and $\pi_a : X \to (B_a, \mathfrak{N}_a)$ an almost toric fibration. Then for any neighbourhood $U \subset B$ of $\pi_B(\mathfrak{N})$, we find a fibration $\pi : X \times I \to B \times I$ such that:*

- $\pi|_{X\times\{a\}} = \pi_a$,
- *for all* $t \in I$, $\pi_t = \pi|_{X\times\{t\}} : X \to (B_t, \mathfrak{N}_t)$ *is an almost toric fibration,*
- *for all* $t \in I$, $X \setminus \pi_t^{-1}(U) = X \setminus \pi_a^{-1}(U)$ *and* $\pi_t|_{X\setminus\pi_a^{-1}(U)} = \pi_a|_{X\setminus\pi_a^{-1}(U)}$.

Using the correspondence Lemma 2.22, this theorem is a direct consequence of [Eva23, Proof of Theorem 8.10]. See also the earlier [Sym03, Theomrem 6.5].

Definition 2.30. Using the notation of Theorem 2.29, we say that we can **lift** a nodal tangle $(B \times I, \mathfrak{N})$ to a path of almost toric fibrations $\pi_t : X \to (B_t, \mathfrak{N}_t)$ **supported** on $U \subset B$.

The following useful lemma shows that although a lift of a nodal tangle modifies the fibres near $\pi_B(\mathfrak{N})$, for any given fibre outside of $\pi_B(\mathfrak{N})$ this can be "undone" by a symplectomorphism:

Lemma 2.31. *Let* $\pi : X \times [0,1] \to (B \times [0,1], \mathfrak{N})$ *be a lift of a nodal tangle. If* B *is homotopy equivalent to a punctured surface, then for all* $x \in B \setminus \pi_B(\mathfrak{N})$ *there exists* $\psi \in \mathrm{Symp}(X)$ *such that* $\pi_0 = \pi_1 \circ \psi$ *near* $\pi_0^{-1}(x)$.

Proof. Extend the nodal tangle by concatenating it with its reverse: set $(B_t, \mathfrak{N}_t) = (B_{2-t}, \mathfrak{N}_{2-t})$ for $t \in [1,2]$, giving a nodal tangle $(B \times [0,2], \mathfrak{N})$.

Let $x \in B \setminus \pi_B(\mathfrak{N})$ and choose a neighbourhood U of $\pi_B(\mathfrak{N})$ such that $x \notin U$. Then by Theorem 2.29 we may lift the nodal tangle $(B \times [1,2], \mathfrak{N})$ to $\pi_t : X \to (B_t, \mathfrak{N}_t), t \in [1,2]$ with the lift being supported on U. In particular we have $\pi_2 = \pi_1$ near x. Since $(B_0, \mathfrak{N}_0) = (B_2, \mathfrak{N}_2)$, applying Theorem 2.26 π_0 and π_2, we get a symplectomorphism $\psi \in \mathrm{Symp}(X)$ such that $\pi_0 = \pi_2 \circ \psi = \pi_1 \circ \psi$ near x. □

Remark 2.32. Taking more care in the proof of Theorem 2.29, it should be possible to build lifts such that the Lagrangian isotopy $t \mapsto \pi_t^{-1}(x), t \in [0,1]$ is generated by a Hamiltonian isotopy, and to get $\psi \in \mathrm{Ham}(X)$ without the restriction on B in Lemma 2.31.

2.4 Nodal tangles and invariant germs

Let $\mathscr{L}$ be the space of Lagrangians in X equipped with the $\mathscr{C}^1$-topology, see [Ono08] for details on the $\mathscr{C}^1$-topology on the space of Lagrangians. Let $\mathscr{I} : \mathscr{L} \to A$ be a symplectic invariant of Lagrangian submanifolds with values in some set A, meaning that for all $\varphi \in \mathrm{Symp}(X)$ and $L \in \mathscr{L}$ we have $\mathscr{I}(\varphi(L)) = \mathscr{I}(L)$.

During a nodal tangle invariants don't change on fibres of $B \setminus \pi_B(\mathfrak{N})$:

Lemma 2.33. *Let* $\pi : X \times I \to (B \times I, \mathfrak{N})$ *be a lift of a nodal tangle, and* $\mathscr{I} : \mathscr{L} \to A$ *a symplectic invariant. If* B *is homotopy equivalent to a punctured surface, then for* $a, b \in I$ *and* $x_a \in B_a \setminus \pi_B(\mathfrak{N})$, $x_b = \tau_a^b x_a$, *we have*

$$\mathscr{I}(\pi_a^{-1}(x_a)) = \mathscr{I}(\pi_b^{-1}(x_b)) \,.$$

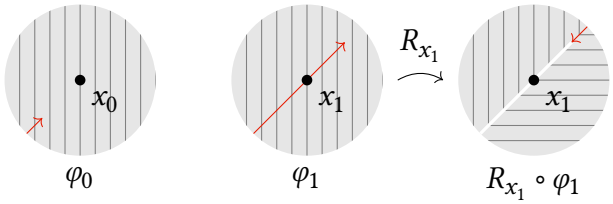

Figure 2.7: Modifying an invariant germ by a simple nodal tangle. We start with a nodal chart φ_0 which is affine around x_0 for B_0, then we modify B_0 by a nodal tangle to obtain B_1 and with $x_1 = \tau_0^1 x_0$, first giving us a nodal chart $\varphi_1 = \varphi_0 \circ \tau_1^0$. We then compose φ_1 with the rectifying map at x to get a nodal chart $R_x \circ \varphi_1$ which is an integral affine chart near x_1. The grey lines are level sets of an invariant $\mathscr{I} : \mathscr{L} \to \mathbb{R}$. The difference of the germs $[\mathscr{I}]_{x_0}$ and $[\mathscr{I}]_{x_1}$ is captured by Corollary 2.34.

Proof. Let $a, b \in I$ and $x \in B \setminus \pi_B(\mathfrak{N})$. Then by Lemma 2.31 there exists $\psi \in \mathrm{Symp}(X)$ such that $\pi_a = \pi_b \circ \psi$ near $\pi_a^{-1}(x)$. In particular $\psi(\pi_a^{-1}(x)) = \pi_b^{-1}(x)$, so

$$\mathscr{I}(\pi_a^{-1}(x)) = \mathscr{I}(\psi(\pi_a^{-1}(x))) = \mathscr{I}(\pi_b^{-1}(x)) \,. \qquad \square$$

For an almost toric fibration $\pi : X \to B$ and a point $x \in B$, abusing notation, denote by $[\mathscr{I}]_x$ the germ of the function $(\mathscr{I} \circ \pi^{-1}) : B^{\mathrm{reg}} := B \setminus (\partial B \cup \mathfrak{N}) \to A$, where we think of π^{-1} as a map $B^{\mathrm{reg}} \to \mathscr{L}$.

While we cannot directly describe how $\mathscr{I}$ changes for points $x \in \pi_B(\mathfrak{N})$ of a nodal tangle, we can partially describe how its germ $[\mathscr{I}]_x$ changes:

Corollary 2.34. *Let $\pi : X \times I \to (B \times I, \mathfrak{N})$ be a lift of a nodal tangle, and $\mathscr{I} : \mathscr{L} \to A$ a symplectic invariant. If B is homotopy equivalent to a punctured surface, then for $a, b \in I$ and $x_a \in B_a$, $x_b = \tau_a^b x_a$, we have*

$$([\mathscr{I}]_{x_a})|_{B_a \setminus \pi_B(\mathfrak{N})} = ([\mathscr{I}]_{x_b} \circ \tau_a^b)|_{B_a \setminus \pi_B(\mathfrak{N})} \,.$$

Remark 2.35. More loosely we can say that $[\mathscr{I}]_{x_a} = [\mathscr{I}]_{x_b} \circ \tau_a^b$ on an open dense neighbourhood of x_a.

Proof. This follows directly from Lemma 2.33 by taking germs. $\square$

See Figure 2.7 for an example.

We can show that the germ $[\mathscr{I}]_x$ only depends on the Lagrangian $\pi^{-1}(x) \subset X$. This requires a bit of setup:

Given a Lagrangian L, using a *versal deformation* $\nu : H^1(L; \mathbb{R}) \to \mathscr{L}$ we can identify a small neighbourhood of L in $\mathscr{L}$ up to local Hamiltonian isotopy with a small neighbourhood of 0 in $H^1(L; \mathbb{R})$. Versal deformations of Lagrangians were introduced in [Che96]. For details we refer the reader to the exposition in [BHS24, Section 3.3]. Denote by $[\mathscr{I}]_L : H^1(L; \mathbb{R}) \dashrightarrow A$ the germ of $\mathscr{I} \circ \nu$ at 0, as defined in

[BHS24, Definition 3.13], which is independent of the choice of versal deformation. This can be considered a refinement of $\mathscr{I}$ by considering values of $\mathscr{I}$ in a small neighbourhood of L.

Let $\pi : X \to (B, \mathfrak{N})$ be an almost toric fibration. For every regular value x of π we have a natural identification $\Lambda_x B \cong H^1(\pi^{-1}(x); \mathbb{Z})$: The map

$$\begin{aligned} \Lambda_x^* B \times H^1(\pi^{-1}(x); \mathbb{Z}) &\to \mathbb{Z} \\ (df, [\alpha]) &\mapsto \omega(X_{\pi^* f}, X_\alpha) \end{aligned}$$

is a perfect pairing, giving an isomorphism $H^1(\pi^{-1}(x); \mathbb{Z}) \cong \Lambda_x B$.[5] This extends to an integral linear isomorphism[6] $\alpha : H^1(\pi^{-1}(x); \mathbb{R}) \to T_x B$. Furthermore, the lattice bundle ΛB induces a flat connection on B such that the exponential map $\exp TB \to B$ locally gives integral affine maps $\exp_x : T_x B \dashrightarrow B$ near $0 \subset T_x B$. (We use $\dashrightarrow$ to denote a map only defined near 0.) Then the composition

$$H^1(\pi^{-1}(x); \mathbb{R}) \xrightarrow{\alpha} T_x B \overset{\exp_x}{\dashrightarrow} B \xrightarrow{\pi^{-1}} \mathscr{L}$$

is a versal deformation. See [BHS24, Section 3.4] for more details.

We summarize the discussion in the following lemma:

Lemma 2.36. *The germ $[\mathscr{I}]_x$ and the invariant germ $[\mathscr{I}]_{\pi^{-1}(x)}$ are related by the commuting diagram*

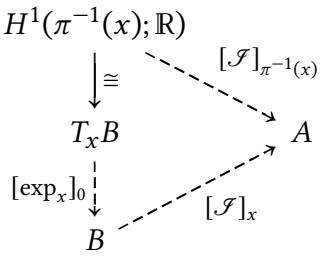

where the vertical maps are integral affine. In particular $[\mathscr{I}]_x$ depends only on the Lagrangian $\pi^{-1}(x)$.

[5] The dual isomorphism $\Lambda_x^* B \to H_1(\pi^{-1}(x); \mathbb{Z})$ has a nice interpretation: It maps an S^1-action in $\Lambda_x^* B$ to the class of its orbit.

[6] Meaning an isomorphism of pairs $\big(H^1(\pi^{-1}(x); \mathbb{R}), H^1(\pi^{-1}(x); \mathbb{Z})\big) \to (T_x B, \Lambda_x B)$.

3 Weakly Delzant polygonal domains

In this section, we combine the framework of Chapter 2 with [MS23] to develop a *canonical form* (Proposition 3.17) for *weakly Delzant polygonal domains*, of which Delzant polygons are important examples. In Section 3.2, we use this canonical form to prove [Symo3, Conjecture 6.8] in the case of closed toric symplectic four-manifolds. In Section 3.4, we use this canonical form and probes introduced in [McD11] to calculate the displacement energy of toric fibres.

3.1 Weakly Delzant polygonal domains and their caustics

For $c \in \mathbb{R}$ and a primitive vector $\lambda \in \mathbb{Z}^2$, define the half-plane

$$H_{\lambda,c} = \{x \in \mathbb{R}^2 \mid \langle \lambda, x \rangle + c \geq 0\} .$$

Definition 3.1. A set $\Delta \subset \mathbb{R}^2$ is a **polygonal domain** if for every compact set $C \subset \mathbb{R}^2$, $\Delta \cap C$ is the intersection of finitely many half-planes and C.

We can write

$$\Delta = \bigcap_{H_{\lambda,c} \in \mathscr{H}} H_{\lambda,c}$$

for a minimal set of half-planes $\mathscr{H}$.

Remark 3.2. $\partial\Delta$ is made up of line segments. The vertices of Δ are isolated, and a small neighbourhood of a vertex may be represented by the intersection of two unique half-planes.

Definition 3.3. For $\lambda \in \mathbb{Z}^n$ write the **greatest common divisor** by

$$\gcd(\lambda) = \max\left\{a \in \mathbb{N}_{>0} \;\middle|\; \frac{1}{a}\lambda \in \mathbb{Z}^n\right\} .$$

Remark 3.4. For all $A \in \mathrm{GL}_n(\mathbb{Z})$, $\gcd(A\lambda) = \gcd(\lambda)$.

Definition 3.5. A vertex x of a polygonal domain Δ is of **type** A_n if the two adjacent half-planes $H_{\lambda_1,c_1}, H_{\lambda_2,c_2}$ satisfy:

$$|\det(\lambda_1, \lambda_2)| = n + 1$$
$$\gcd(\lambda_1 - \lambda_2) = n + 1 \,,$$

with $n \in \mathbb{Z}_{\geq 0}$. We call x **weakly Delzant** if there exists $n \in \mathbb{Z}_{\geq 0}$ such that x is of type A_n.

We say that Δ is **weakly Delzant** if all vertices of Δ are weakly Delzant. We say that Δ is **Delzant** if all vertices of Δ are of type A_0.

In [MS23], weakly Delzant polygonal domains are called *canonical tropical domains*.

Remark 3.6. A polygonal domain is an integral affine surface (with corners) if and only if it is Delzant.

Remark 3.7. If Δ is weakly Delzant, there is a unique symplectic toric orbifold with moment map $\mu : \tilde{X} \to \Delta$. An A_n-type vertex of Δ is the image of an A_n-singular point of μ in $\tilde{X}$, see [Eva23, Section 3.4] for details.

Let $\Delta \subset \mathbb{R}^2$ be a weakly Delzant polygonal domain, and write $\Delta = \bigcap_{H_{\lambda,c} \in \mathscr{H}} H_{\lambda,c}$, where $\mathscr{H}$ is a minimal set of half-planes. Let

$$\begin{aligned} \mathscr{F}_\Delta : \mathbb{R}^2 &\to \mathbb{R} \cup \{-\infty\} \\ p &\mapsto \inf_{H_{\lambda,c} \in \mathscr{H}} \{\langle \lambda, p \rangle + c\} \,, \end{aligned}$$

be the **height function** of Δ. We can write $\Delta = \mathscr{F}_\Delta^{-1}(\{s \geq 0\})$. For $t \in \mathbb{R}$, set $\Delta_t = \mathscr{F}_\Delta^{-1}(\{s \geq t\}) = \bigcap_{H_{\lambda,c} \in \mathscr{H}} H_{\lambda,c+t}$. See Figure 3.1.

The value $-\infty$ is never attained by $\mathscr{F}_\Delta$, as by Definition 3.1 only finitely many half-planes contribute to the infimum.

Definition 3.8. The **caustic** $\mathscr{K}_\Delta$ **of** Δ is the set of points of Δ where $\mathscr{F}_\Delta$ is not affine. See Figure 3.1.

Remark 3.9. The caustic $\mathscr{K}_\Delta$ is a tropical curve: By Definition 3.1, the restriction of $\mathscr{F}_\Delta$ to any compact set is a tropical polynomial. See e.g. [BS14, Section 2.1] for the definition of a tropical curve.

Theorem 3.10 ([MS23, Theorem 26])**.** *Let Δ be weakly Delzant. Then Δ_t is a weakly Delzant polygonal domain for all $0 \leq t < \sup \mathscr{F}_\Delta$.*

Definition 3.11. We say that an edge ℓ of $\mathscr{K}_\Delta$ has **weight** n if for any x in the interior of ℓ, x is an A_{n-1}-type vertex of the weakly Delzant polygonal domain $\Delta_{\mathscr{F}_\Delta(x)}$.

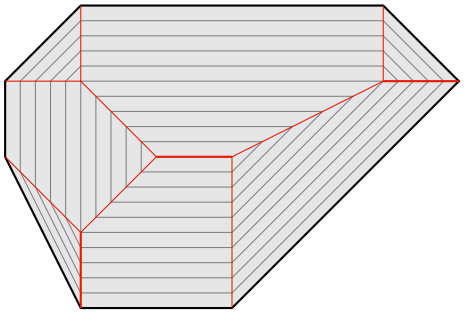

Figure 3.1: Level sets of $\mathscr{F}_\Delta$ in dark grey and the caustic $\mathscr{K}_\Delta$ in red.

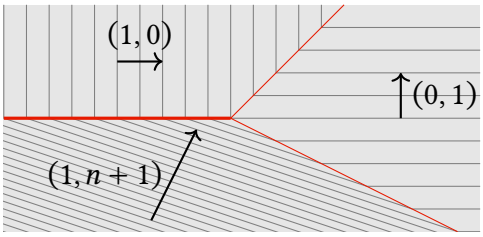

Figure 3.2: Level sets of $\mathscr{F}_\Delta$ near a vertex of $\mathscr{K}_\Delta$ outside of Δ_M.

Remark 3.12. For edges where the weight is defined (namely those not contained in the max-set of $\mathscr{F}_\Delta$), this is equal to the weight of an edge of a tropical curve given by a tropical polynomial, see for example [BS14, Definition 2.1].

The following theorem describes the local behaviour of $\mathscr{F}_\Delta$ near edges and vertices of $\mathscr{K}_\Delta$. For edges, this is a reformulation of Theorem 3.10, while the statement for vertices is a reformulation of [MS23, Theorem 46].

Theorem 3.13 ([MS23, Theorems 26, 46])**.** *Let Δ be weakly Delzant and $M = \sup \mathscr{F}_\Delta$. If ℓ is an edge of $\mathscr{K}_\Delta$ in $\Delta \setminus \Delta_M$ of weight $n+1$, x is in the interior of ℓ and $a \in \mathbb{R}^2$ small enough, then, after an integral affine transformation, we can write*

$$\mathscr{F}_\Delta(x+a) = \mathscr{F}_\Delta(x) + \min\{\langle (1,0), a\rangle, \langle (1, n+1), a\rangle\}\,.$$

For a vertex x of $\mathscr{K}_\Delta$ in $\Delta \setminus \Delta_M$ and $a \in \mathbb{R}^2$ small enough, after an integral affine transformation, we can write

$$\mathscr{F}_\Delta(x+a) = \mathscr{F}_\Delta(x) + \min\left\{\langle (1,0), a\rangle, \langle (1, n+1), a\rangle, \langle (0,1), a\rangle\right\}$$

with $n \in \mathbb{Z}_{\geq 0}$.

The case of a vertex is illustrated in Figure 3.2.

Corollary 3.14. *If Δ is a Delzant polygonal domain, then so is Δ_t for all $0 \leq t < \sup \mathscr{F}_\Delta$ and in Theorem 3.13 we have $n = 0$ for all vertices and edges of $\mathscr{K}_\Delta$.*

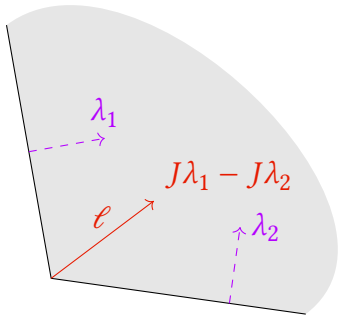

Figure 3.3: Smoothing an A_n corner.

Definition 3.15. We can **smooth** an A_n type vertex x of a weakly Delzant polygonal domain by decorating it as follows: Let $H_{\lambda_1,c_1}, H_{\lambda_2,c_2}$ be the two incident half planes at x with $\det(\lambda_1, \lambda_2) = n+1$, and let J be the rotation by $\pi/2$. We add a small cut ℓ from x in direction $J(\lambda_1 - \lambda_2)$ ending in a node $\mathfrak{n}$ of multiplicity $n+1$.

By interpreting this as a nodal chart diagram, this makes Δ into a nodal integral affine surface near x.

Let Δ be a weakly Delzant polygonal domain with exactly one vertex x. Smooth x to obtain a nodal integral affine surface $(B, \{\mathfrak{n}\})$ with a simple nodal chart $\varphi : B \to \Delta$ with nodal chart diagram given by Definition 3.15. Since B is contractible, by Theorem 2.26, it determines a unique symplectic manifold X with an almost toric fibration $\pi : X \to B$. We also can obtain X by smoothing the A_n singularity corresponding to the vertex x of the toric orbifold $\mu : \tilde{X} \to \Delta$ determined by Remark 3.7 as in [Eva23, Section 7.3]. For a neighbourhood U of the cut ℓ, we can also require that the fibrations $\varphi \circ \pi : X \setminus (\varphi \circ \pi)^{-1}(U) \to \Delta$ and $\mu : \tilde{X} \setminus \mu^{-1}(U) \to \Delta$ are identical. If $n = 0$, the A_0 singularity is smooth already and the smoothing corresponds to a *nodal trade* (see [Sym03, Lemma 6.3] or [Eva23, Section 8.2]), and we have $X = \tilde{X}$.

Remark 3.16. The cut ℓ obtained by smoothing a vertex x lies in the caustic $\mathscr{K}_\Delta$: Near x the caustic is given by the equation

$$\langle \lambda_1, \cdot \rangle + c_1 = \langle \lambda_2, \cdot \rangle + c_2 \Leftrightarrow \langle \lambda_1 - \lambda_2, \cdot \rangle + c_1 - c_2 = 0$$

and by construction ℓ is contained in this set. In particular, by modifying the nodal integral affine surface B by small nodal slides of $\mathfrak{n}$, the node stays on the caustic.

Proposition 3.17. *Let $(B_0, \mathfrak{N}_0)$ be the nodal integral affine surface obtained by smoothing all vertices of a weakly Delzant polygonal domain Δ, and let $\varphi_0 : B_0 \to \Delta$ be the associated nodal chart.*

For any $0 < M_\varepsilon < M := \sup \mathscr{F}_\Delta$ there exists a nodal tangle $(B \times [0,1], \mathfrak{N})$ starting at $(B_0, \mathfrak{N}_0)$ such that $\mathscr{F}_1 := \mathscr{F}_\Delta \circ \varphi_1$ is an integral affine function on $B_1 \setminus (\varphi_1^{-1}(\Delta_{M_\varepsilon}) \cup \mathfrak{N}_1)$, where $\varphi_1 := \varphi_0 \circ \tau_1^0$.

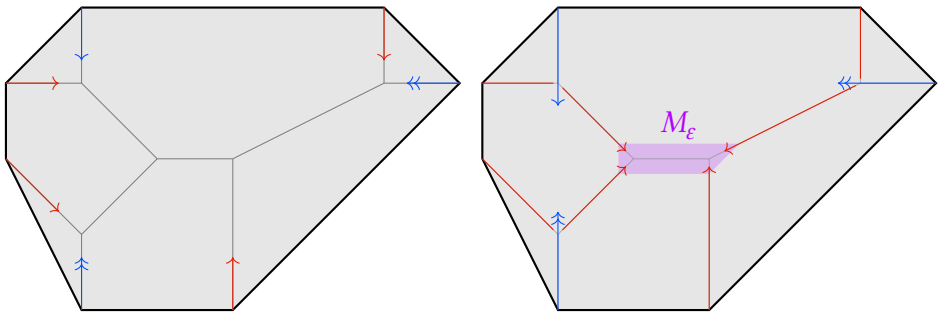

Figure 3.4: a): smoothing a weakly Delzant polygon Δ.
b): filling the caustic $\mathscr{K}_\Delta$ with cuts.
Nodes of multiplicity 2 have a double arrow head. Nodes parked in b) and their cuts are drawn in blue.

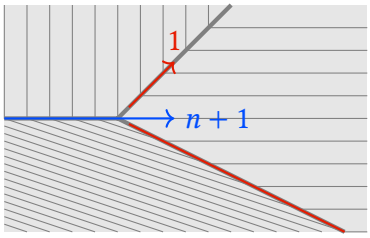

Figure 3.5: Filling $\mathscr{K}_\Delta$ with cuts near a vertex of $\mathscr{K}_\Delta$.

In applications we take M_ε to be arbitrarily close to M.

Proof. To construct the nodal tangle $(B \times [0,1], \mathfrak{N})$ we proceed as illustrated in Figure 3.4 b): By Remark 3.16 all nodes introduced by the smoothing slide on the caustic. Sort the nodes by decreasing multiplicity. Start with the node $\mathfrak{n}_1$ and slide it up (with respect to the height function $\mathscr{F}_\Delta$) until it slides off the caustic at a vertex of $\mathscr{K}_\Delta$, or it is contained in Δ_{M_ε}. If it slides off $\mathscr{K}_\Delta$ at a vertex we stop it shortly after the vertex and call it **parked**. Now continue with the next node $\mathfrak{n}_2$. If it reaches a vertex x of $\mathscr{K}_\Delta$ where a node previously slid off $\mathscr{K}_\Delta$, Theorem 3.13 assures that the multiplicity of $\mathfrak{n}_2$ is 1 and, using Remark 2.19, $\mathfrak{n}_2$ stays on $\mathscr{K}_\Delta$ sliding through x. See Figure 3.5. Continuing this procedure, we see inductively that every node either becomes parked or stays on the caustic and eventually ends up in Δ_{M_ε}. This procedure provides a nodal tangle $(B \times [0,1], \mathfrak{N})$.

Now we show that $\mathscr{F}_1 : (B_1, \mathfrak{N}_1) \to \mathbb{R}$ is integral affine on $B_1 \setminus (\varphi_1^{-1}(\Delta_{M_\varepsilon}) \cup \mathfrak{N}_1)$.

Let G be the cut graph of φ_1^{-1} in $\Delta \setminus \Delta_{M_\varepsilon}$. By construction of $(B_1, \mathfrak{N}_1)$ we have $\mathscr{K}_\Delta \cap (\Delta \setminus \Delta_{M_\varepsilon}) \subset G$ and that $\mathscr{F}_1$ is integral affine on $\varphi_1^{-1}(\Delta \setminus (\Delta_{M_\varepsilon} \cup G))$.

Let $\varphi_1(x) \in G \setminus \varphi_1(\mathfrak{N}_1)$. Then $\varphi_1(x)$ is either in the interior of an edge ℓ of $\mathscr{K}_\Delta$, a

vertex of $\mathscr{K}_\Delta$ or in the interior of a cut of G connecting a vertex of $\mathscr{K}_\Delta$ to a parked node.

Suppose $\varphi_1(x) \in \mathscr{K}_\Delta$ is a vertex of $\mathscr{K}_\Delta$ and, after a translation of Δ, $\varphi_1(x) = 0$. See Figure 3.5. After an integral affine transformation, using Theorem 3.13 and the construction of the nodal tangle $(B \times [0,1], \mathfrak{N})$,

$$\mathscr{F}_\Delta(\underbrace{\varphi_1(x)}_{=0} + a) = \mathscr{F}_\Delta(a) = \mathscr{F}_1(x) + \min\{\langle (1,0), a\rangle, \langle (1, n+1), a\rangle, \langle (0,1), a\rangle\} \tag{3.1}$$

$$R_0 = h_{(1,n+1)} \circ h_{(1,0)}^{n+1} ,$$

where R_0 is the rectifying map at 0 of φ_1, and h_v denotes a half-shear as in (2.1) Taking the integral affine chart $R_0 \circ \varphi_1$, using (3.1) and applying the half-shears of R_0 to Figure 3.5, it is quickly verified that for small $a \in \mathbb{R}^2$,

$$(\underbrace{\mathscr{F}_\Delta \circ \varphi_1}_{=\mathscr{F}_1} \circ (R_0 \circ \varphi_1)^{-1})(a) = \mathscr{F}_\Delta(R_0^{-1} a) = \mathscr{F}_1(x) + \langle (1,0), a\rangle ,$$

showing that $\mathscr{F}_1 = \mathscr{F}_\Delta \circ \varphi_1$ is affine linear near x.

We proceed similarly in the remaining two cases. □

Remark 3.18. We may choose a different nodal chart for $(B_1, \mathfrak{N}_1)$ of Proposition 3.17 in which $\mathscr{F}_1$ is visibly integral affine:

Take the annulus $A = \varphi_1^{-1}(\Delta \setminus \Delta_M) \subset (B_1, \mathfrak{N}_1)$, and remove a straight line ℓ such that $U = A \setminus \ell$ is simply connected. On U we may choose a nodal chart φ' as in Figure 3.6 as follows: The level sets $\mathscr{F}_1^{-1}(h)$ with $h \le M_\varepsilon$ are all straight lines. For $x \in B_1$ and $h = \mathscr{F}_1(x)$, let $f(x)$ be the integral affine length of $\mathscr{F}_\Delta^{-1}(h)$ between $\mathscr{F}_\Delta^{-1}(h) \cap \ell$ and x in the counter-clockwise direction. Then $\varphi' = (f, \mathscr{F}_1)$ is a nodal chart of $B_1 \setminus (\ell \cup \varphi_0^{-1}(\Delta_M))$. See Figure 3.6.

In this nodal chart the parked nodes have horizontal cuts. Hence $\mathscr{F}_1$ is indeed integral affine on $A \setminus \mathfrak{N}_1$.

3.2 Toric actions on symplectic four manifolds

Theorem 3.13 describes vertices x of $\mathscr{K}_\Delta$ with $\mathscr{F}_\Delta(x) < \sup \mathscr{F}_\Delta$. [MS23, Propositions 54, 55] describe vertices x of $\mathscr{K}_\Delta$ with $\mathscr{F}_\Delta(x) = \sup \mathscr{F}_\Delta$. Here we restate the case of Delzant polygonal domains:

Proposition 3.19. *Let Δ be a Delzant polygonal domain. Then near a vertex x of $\mathscr{K}_\Delta$ with $\mathscr{F}_\Delta(x) = \sup \mathscr{F}_\Delta$, up to an integral affine transformation, $\mathscr{F}_\Delta$ is given by one of the seven possibilities in Figure 3.7.*

Let Δ be a compact Delzant polygonal domain. Since then $M = \sup \mathscr{F}_\Delta < \infty$, we may choose $M_\varepsilon = M - \varepsilon$ such that $\Delta_{M_\varepsilon} \setminus \Delta_M$ contains no vertices of $\mathscr{K}_\Delta$.

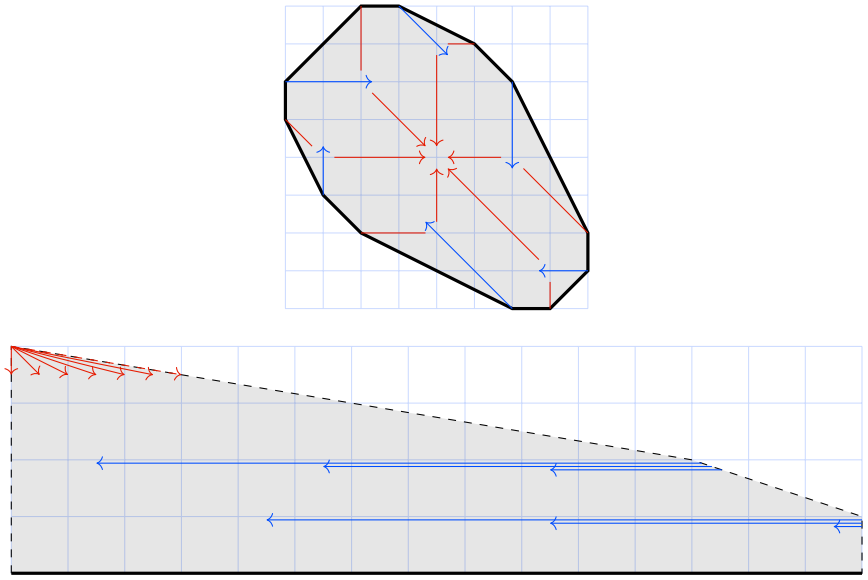

Figure 3.6: Constructing an "open" nodal chart. Parked nodes are drawn in blue.

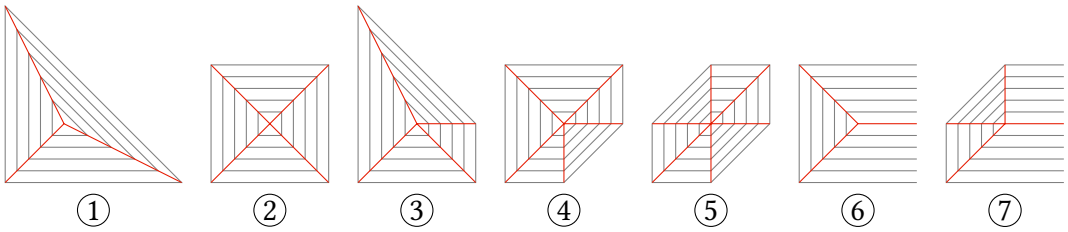

Figure 3.7: Possible caustics near $\sup \mathscr{F}_\Delta$ for Delzant polygonal domains. $\mathscr{K}_\Delta$ in red, level sets of $\mathscr{F}_\Delta$ in grey.

Definition 3.20. In this case we call B_1 as constructed in Proposition 3.17 the **canonical form** of Δ. The ε**-hat** of B_1 is given by the nodal integral affine surface

$$H_\varepsilon = \{x \in B_1 \mid \mathscr{F}_1(x) > M - \varepsilon\}\,.$$

The **hat width** is given by the integral affine length of Δ_M.

Definition 3.21. An ε_1-hat H_1 is equivalent to an ε_2-hat H_2 if, after a nodal tangle, $H_1 \subset H_2$ or $H_2 \subset H_1$. We call the equivalence class of an ε-hat its **hat class**.

Lemma 3.22. *There are*

- *five hat classes of width* $w = 0$,
- *four hat classes of width* $w > 0$.

They are listed in Figure 3.8.

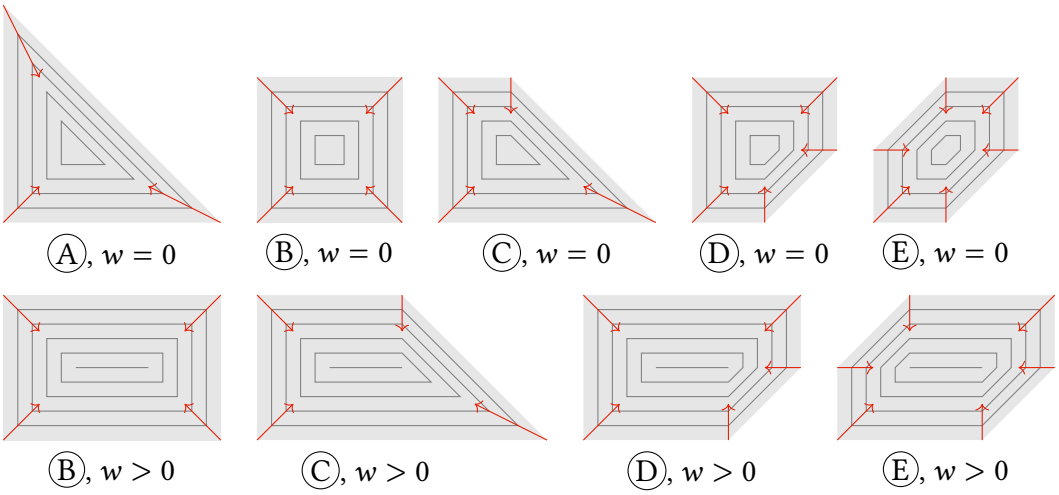

Figure 3.8: All possible ε-hats up to nodal tangle.

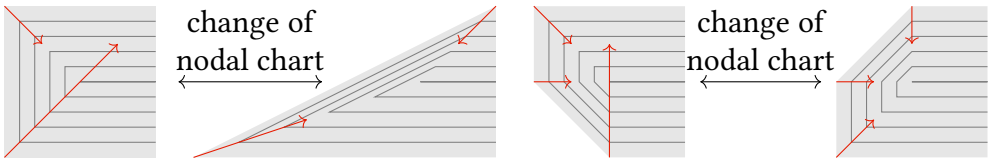

Figure 3.9: Nodal tangle transforming part of an ε-hat of positive width.

Proof. If $w = 0$, this follows immediately from Proposition 3.19, with the five hats Ⓐ–Ⓔ in the top row of Figure 3.8 corresponding to the caustics ①–⑤ in Figure 3.7.

If $w > 0$, then the ε-hat must be assembled from ⑥ and ⑦ in Figure 3.7, and it is easy to check that there exists a nodal tangle relating it to one of the ε-hats in the bottom row of Figure 3.8. See Figure 3.9. □

Definition 3.23. The **canonical type** of a compact Delzant polygonal domain Δ is given by $(H, M, \alpha_1, ..., \alpha_n)$, where

- H is the hat class of an ε-hat of Δ,
- $M = \sup \mathscr{F}_\Delta$,
- $\alpha_i = \mathscr{F}_1(\mathfrak{a}_i)$ where $\mathfrak{a}_1, ..., \mathfrak{a}_n$ are the parked nodes of $(B_1, \mathfrak{N}_1)$ such that $\alpha_1 \geq \alpha_2 \geq ... \geq \alpha_n$.

We can reconstruct the canonical form of Δ from its canonical type up to nodal tangle. In Figure 3.6 the α_i's correspond to the heights of the parked nodes.

Definition 3.24 ([KK17, Definition 1.2])**.** Let $k \in \mathbb{Z}_{\geq 0}$. A vector $v = (\lambda, \delta_1, ..., \delta_k) \in \mathbb{R}^{k+1}$ is **reduced** if

$$\delta_1 \geq \delta_2 \geq ... \geq \delta_k, \quad \delta_1 + \delta_2 + \delta_3 \leq \lambda \, .$$

If additionally

$$\delta_1 \geq \delta_2 \geq \ldots \geq \delta_k > 0 \quad \text{and} \quad \lambda^2 - \sum_{i=1}^{k} \delta_i^2 > 0 \,,$$

we call it **symplectic**.

Let $X_k = \mathbb{C}P^2 \# k\overline{\mathbb{C}P^2}$. In [KK17] it is shown that symplectic reduced vectors classify symplectic forms ω on X_k up to diffeomorphism. In a symplectic reduced vector, λ encodes the symplectic size of $\mathbb{C}P^2$, and the δ_i encode the symplectic sizes of the blow-ups used to obtain X_k from $\mathbb{C}P^2$. For a reduced vector v denote by ω_v the corresponding symplectic form.

We call a symplectic reduced vector v **toric** if the corresponding (X, ω_v) admits a toric moment map.

Let $\mathscr{R}$ be the set of all toric reduced vectors, and let $\mathscr{C}$ be the set of all canonical types obtained from compact Delzant polygonal domains.

Theorem 3.25. *There is a bijection $\alpha : \mathscr{C} \to \mathscr{R}$ such that if $\mu : (X, \omega_v) \to \Delta$ is a toric moment map, the canonical type of Δ is sent to v.*

In particular, every four-manifold admitting a toric moment map has a unique canonical type.

Proof. Take $C = (H, M, \alpha_1, \ldots, \alpha_n) \in \mathscr{C}$ and let w be the width of H. Depending on the hat class H we define $\alpha(C)$ as follows:

H	λ,	$\delta_1, \ldots, \delta_k$
Ⓐ	$3M$,	$\alpha_1, \ldots, \alpha_n$
Ⓑ	$4M + w - \alpha_1$,	$(2M + w - \alpha_1), (2M - \alpha_1), \alpha_2, \ldots, \alpha_n$
Ⓒ	$3M + w$,	$M + w, \alpha_1, \ldots, \alpha_n$
Ⓓ	$3M + w$,	$M + w, M, \alpha_1, \ldots, \alpha_n$
Ⓔ	$3M + w$,	$M + w, M, M, \alpha_1, \ldots, \alpha_n$

(We used the same letters as in Figure 3.8 to denote the type of hat.) The rest of the proof will motivate this definition. It is easy to check that in each case the vector $\alpha(C)$ is reduced and symplectic: The inequalities $\delta_1 \geq \ldots \geq \delta_k > 0$ and $\delta_1 + \delta_2 + \delta_3 \leq \lambda$ are quickly verified using $M > \alpha_1 \geq \alpha_2 \geq \ldots \geq \alpha_n$ and $w \geq 0$. Moreover, the quantity $\lambda^2 - \sum_{i=1}^{k} \delta_i^2$ is equal to twice the area of B, which is positive. This can be most easily verified by examining a nodal chart diagram as in Remark 3.18, which we do for the hat type Ⓔ, as pictured in Figure 3.6 in the case $w = 0$. For the case Ⓔ we have

$$\lambda^2 - \sum_{i=1}^{k} \delta_i^2 = (3M + w)^2 - (M + w)^2 - 2M^2 - \sum_{i=1}^{n} \alpha_i^2 = 6M^2 + 4Mw - \sum_{i=1}^{n} \alpha_i^2 \,. \quad (3.2)$$

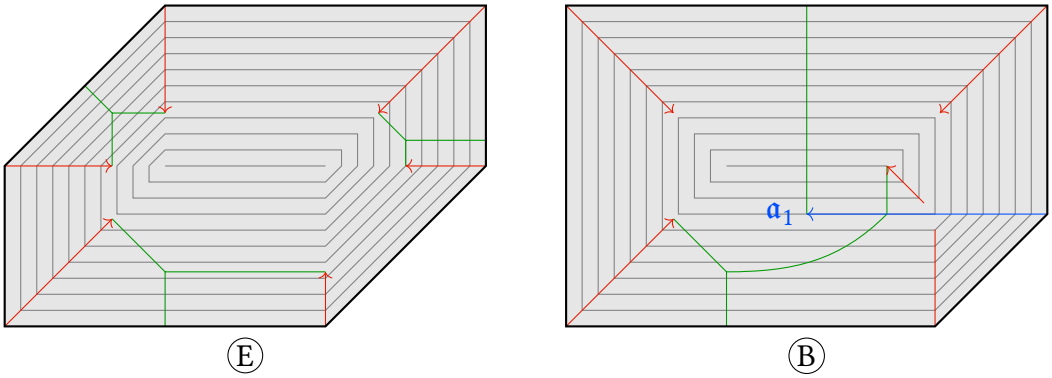

Figure 3.10: Visible tropical spheres for hats of type Ⓔ and Ⓑ.

If there were no parked nodes, Figure 3.6 would be the union of a triangle of height M and width $6M$ and a rectangle of height M and width $2w$. Every time we introduce a parked node we remove $\alpha_i^2/2$ area, so twice the area of B is given by the right hand side of (3.2).

Let $(B, \mathfrak{N})$ be the canonical form given by C and $\pi : (Y, \omega) \to (B, \mathfrak{N})$ an almost toric fibration. Our goal is to show that (Y, ω) is symplectomorphic to (X, ω_v) for some reduced vector v uniquely determined by C. We proceed as follows: To start, suppose for simplicity that H is not of type Ⓑ. First, we blow down (Y, ω) symplectically with sizes $\alpha_n, ..., \alpha_1$. This can be done either as *almost toric blow downs* ([Eva23, Section 9.1]) at the parked nodes $\mathfrak{a}_n, ..., \mathfrak{a}_1$, or as blow downs along the exceptional *visible symplectic spheres* obtained by connecting $\mathfrak{a}_n, ..., \mathfrak{a}_1$ to ∂B by smooth paths transversal to the height function $\mathscr{F}_1$. In this manner we arrive at an almost toric base diagram without parked nodes. Pushing the remaining nodes to the boundary, we get a toric base diagram. Depending on H, the resulting symplectic space is

Ⓐ	Ⓒ	Ⓓ	Ⓔ
$\mathbb{C}P^2$	$\mathbb{C}P^2\#\overline{\mathbb{C}P^2}$	$\mathbb{C}P^2\#2\overline{\mathbb{C}P^2}$	$\mathbb{C}P^2\#3\overline{\mathbb{C}P^2}$

Blowing down up to three more times with appropriate sizes (see the table above), we get $\mathbb{C}P^2$. The symplectic exceptional spheres along which we blow down can be seen as *visible tropical symplectic curves* ([CV22, Section 4.1]), see Figure 3.10 for the hat type Ⓔ. In total, we see that all symplectic spheres along which we blow down can be chosen to be disjoint — indeed, they are all visible in B as disjoint visible (tropical) symplectic curves — and the sequence of blow down sizes produces a symplectic reduced vector $\alpha(C)$ as in the table above. Thus $(V, \omega) = (X, \omega_v)$.

For the case of a hat H of type Ⓑ, we only blow down $\alpha_n, ..., \alpha_2$, arriving at $\mathbb{C}P^2\#2\overline{\mathbb{C}P^2}$. Blowing down two more times with appropriate sizes (see the table above), we get $\mathbb{C}P^2$. The exceptional visible tropical spheres can be seen in Fig-

ure 3.10. (Here we need to avoid blowing down α_1, as otherwise we get stuck at $S^2 \times S^2$.)

The size λ of $\mathbb{C}P^2$ thusly obtained can be calculated from H and M (and α_1 in the case of a hat of type Ⓑ).

To show that this gives a one-to-one correspondence, we construct an inverse $\beta : \mathscr{R} \to \mathscr{C}$. Given $\lambda, \delta_1, ..., \delta_k$, set

$$M = \min\left\{\frac{\lambda}{3}, \frac{\lambda - \delta_1}{2}\right\} = \begin{cases} \frac{\lambda}{3} & \text{if } \frac{\lambda}{3} \geq \delta_1 \\ \frac{\lambda - \delta_1}{2} & \text{if } \delta_1 \geq \frac{\lambda}{3} \end{cases}.$$

Depending on how many δ_i are bigger or equal than M, we define the canonical type $\beta(\lambda, \delta_1, ..., \delta_k) = (H, M, \alpha_1, ..., \alpha_n)$ as follows:

	H	$\alpha_1, ..., \alpha_n$
$M > \delta_1$	Ⓐ, $w = 0$	$\delta_1, ..., \delta_k$
$\delta_1 \geq \delta_2 > M > \delta_3$	Ⓑ, $w = \delta_1 - \delta_2$	$(\lambda - \delta_1 - \delta_2), \delta_3, ..., \delta_k$
$\delta_1 \geq M > \delta_2$	Ⓒ, $w = \frac{3\delta_1 - \lambda}{2}$	$\delta_2, ..., \delta_k$
$\delta_1 \geq \delta_2 = M > \delta_3$	Ⓓ, $w = \frac{3\delta_1 - \lambda}{2}$	$\delta_3, ..., \delta_k$
$\delta_1 \geq \delta_2 = \delta_3 = M > \delta_4$	Ⓔ, $w = \frac{3\delta_1 - \lambda}{2}$	$\delta_4, ..., \delta_k$

(This table can be constructed by following the above process in reverse, starting with $\mathbb{C}P^2$ and performing toric blow-ups for all $\delta_i \geq M$, then reading off the hat type.) It is easily checked that $\beta \circ \alpha = \mathrm{id}_{\mathscr{C}}$ and $\alpha \circ \beta = \mathrm{id}_{\mathscr{R}}$. □

Corollary 3.26. *Let $\mu_i : X \to \Delta_i$ with $i \in \{1, 2\}$ be two toric moment maps on a four dimensional closed symplectic manifold. Then smoothings (Definition 3.15) of Δ_1 and Δ_2 are connected by a nodal tangle.*

Proof. Since the canonical type is uniquely determined by X (Theorem 3.25), both Δ_1 and Δ_2 have the same canonical form, and are thus their smoothings are connected by a nodal tangle. □

See Section 5.2 for possible generalizations.

3.3 Lagrangian Poincaré non-recurrence

The goal of this section is to prove Theorem B. That is, for a compact non-monotone toric symplectic four manifold (X, ω), we want to construct a Lagrangian $L \subset (X, \omega)$ and Hamiltonian diffeomorphism ψ such that $\psi^n(L) \cap L = \emptyset$ for all $n \in \mathbb{Z}_{>0}$.

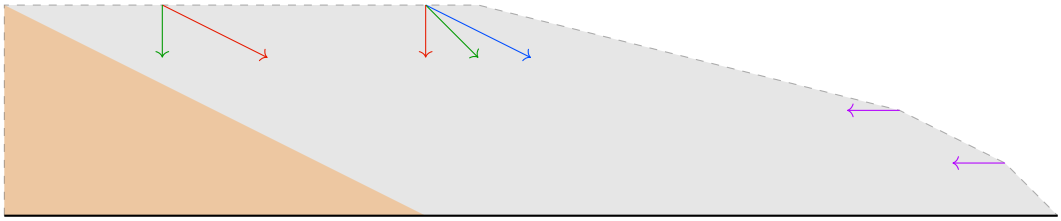

a) Nodal chart diagram for φ_0

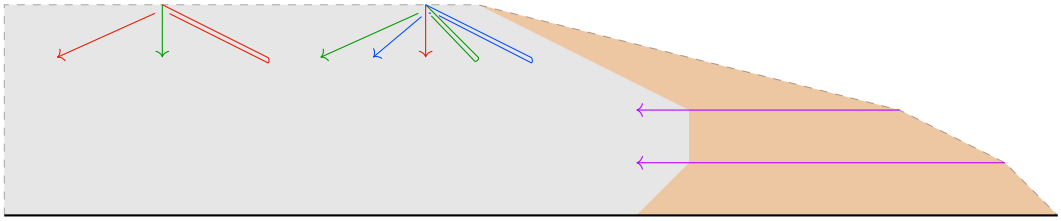

b) Nodal chart diagram for φ_1

Figure 3.11: Two nodal charts for the same canonical type.

Proof of Theorem B. We give the proof in three parts:

The base space. Let $(B_0, \mathfrak{N}_0)$ be a nodal integral affine surface for (X, ω) as in Proposition 3.17 with canonical type $(H, M, \alpha_1, ..., \alpha_n)$ obtained by modifying a Delzant polygon by a nodal tangle. Recall that $(B_0, \mathfrak{N}_0)$ admits a natural nodal chart $\varphi_0 : B_0 \to \mathbb{R}^2$ as in Remark 3.18, illustrated in Figure 3.11 a). Let $\mathscr{F} : B_0 \to [0, M)$ be the height function on B_0 inherited from the Delzant polygon and let $\varepsilon > 0$. We may choose the nodes in the hat H to have at least height $M - \varepsilon$. The level sets $\mathscr{F}^{-1}(h)$ with $h \in [0, M - \varepsilon)$ are closed straight lines in B_0. We have $M = \max \mathscr{F}$, and we call $\Delta_M := \mathscr{F}^{-1}(M)$ the **ridge** of B_0. The integral affine length of Δ_M is the width w of the hat H (Definition 3.20). The integral affine length of $\mathscr{F}^{-1}(h)$ is given by the function

$$\begin{aligned} g : \mathbb{R} &\to \mathbb{R} \\ h &\mapsto 2w - k(M - h) + \sum_{i=1}^{n} \min\{h - \alpha_i, 0\}, \end{aligned}$$

where k is a constant depending on the hat class of H as follows:

Ⓑ	Ⓒ	Ⓓ	Ⓔ
$k = 8$	$k = 8$	$k = 7$	$k = 6$

where we used the same notation as in Figure 3.8.

The nodal tangle. If $n > 0$, B_0 has at least one parked node. Let $\mathfrak{a}_n$ be a parked node with smallest height $\alpha_n = \mathscr{F}(\mathfrak{a}_n)$. Sliding $\mathfrak{a}_n$ once around the curve $\mathscr{F}^{-1}(\alpha_n)$ gives

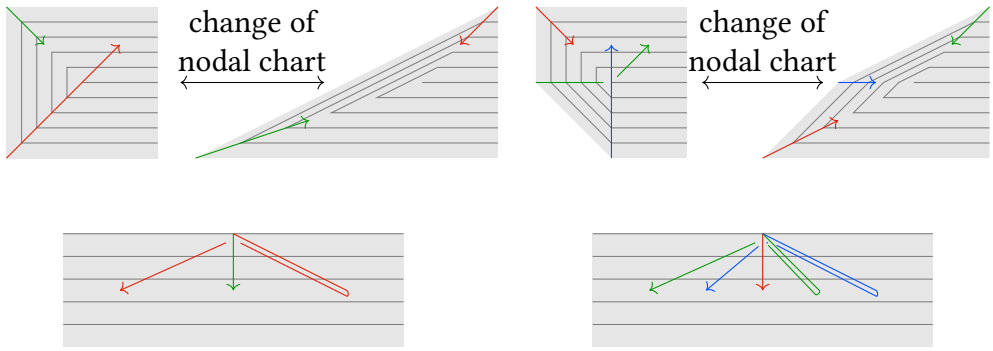

Figure 3.12: Nodal tangle transforming part of an ε-hat of positive width. On the left the nodal tangle for an end of Δ_M with two incoming nodes, on the right the one for an end with three incoming nodes. The top row shows the nodal tangle in a nodal chart as in Figure 3.8, the bottom row shows the same nodal tangle in a nodal chart as in Figure 3.11.

us the construction alluded to in [Sch24, Remark 3.2] leading to a counterexample to the Lagrangian Poincaré recurrence conjecture.

Here we give a different approach that provides slightly different examples. Suppose that the hat H has width $w > 0$. Then H contains the line segment Δ_M. As can be seen from Figure 3.8, there are two types of ends of Δ_M: either there are three nodes pointing to the end or two. Depending on the types of ends of Δ_M, modify H by a nodal tangle as in Figure 3.12. Let $\mathfrak{a}_1, ..., \mathfrak{a}_n$ be the parked nodes of B_0 with height $\mathscr{F}(\mathfrak{a}_i) = \alpha_i$. Further modify B_0 by a nodal tangle by sliding each parked node $\mathfrak{a}_i$ to the left by $2(M - \alpha_i)$. Denote by $(B_1, \mathfrak{N}_1)$ the resulting nodal integral affine surface, and by $(B \times [0,1], \mathfrak{N})$ the nodal tangle connecting $(B_0, \mathfrak{N}_0)$ to $(B_1, \mathfrak{N}_1)$. We also get the natural nodal chart $\varphi_1 : (B_1, \mathfrak{N}_1) \to \mathbb{R}^2$ as in Figure 3.11 b). There is a integral affine isomorphism $\tau : (B_0, \mathfrak{N}_0) \to (B_1, \mathfrak{N}_1)$: The nodal chart diagrams in Figure 3.11 a) and b) of $(B_0, \mathfrak{N}_0)$ and $(B_1, \mathfrak{N}_1)$ are related by applying the shear matrix $\left(\begin{smallmatrix} 1 & 2 \\ 0 & 1 \end{smallmatrix}\right)$ to Figure 3.11 a) and cutting the orange triangle off Figure 3.11 a) and regluing it as indicated in Figure 3.11 b). We quickly verify that this indeed gives an integral affine isomorphism: For points in the interior of the nodal chart diagrams in Figure 3.11 this is obvious. For points in a neighbourhood of Δ_M this can be verified in a nodal chart as in Figure 3.12.

The Hamiltonian diffeomorphism. Let U be an ε-neighbourhood in $[0, M]$ of the points $\{M, \alpha_1, ..., \alpha_n\}$. Then we have $\mathscr{F}(\pi_B(\mathfrak{N})) \subset U$. Let $\pi : X \times [0,1] \to (B \times [0,1], \mathfrak{N})$ be a lift of the nodal tangle $(B \times [0,1], \mathfrak{N})$ supported on $\mathscr{F}^{-1}(U)$ (Theorem 2.29). The symplectic manifold X is determined by $(H, M, \alpha_1, ..., \alpha_n)$, see Theorem 3.25. Since τ is an integral affine isomorphism identifying B_0 and B_1,

Theorem 2.26 gives a symplectomorphism $\psi \in \mathrm{Symp}(X)$ such that

$$\begin{array}{ccc} X & \xrightarrow{\psi} & X \\ \downarrow{\scriptstyle \pi_0} & & \downarrow{\scriptstyle \pi_1} \\ (B_0, \mathfrak{N}_0) & \xrightarrow{\tau} & (B_1, \mathfrak{N}_1) \end{array}$$

commutes outside of the set $\mathscr{F}^{-1}(U)$. Let $x \in \mathscr{F}^{-1}([0, M] \setminus U)$ in B_0, and $h = \mathscr{F}(x)$ its height. Then $\psi(\pi_0^{-1}(x)) = \pi_1^{-1}(\tau(x)) = \pi_0(2(M-h) \cdot x)$, where $t\cdot$ denotes the $\mathbb{R}$-action on $B_0 \setminus \Delta_M$ translating a point x by integral affine distance t in the clockwise direction along the level set $\mathscr{F}^{-1}(h)$. The level set $\mathscr{F}^{-1}(h)$ has integral affine length $g(h)$, so for $x \in \mathscr{F}^{-1}([0, M] \setminus U)$ with $\frac{g(h)}{2(M-h)}$ irrational we have $\psi^n(\pi_0^{-1}(x)) \cap \pi_0^{-1}(x) = \emptyset$ for all $n \geq 0$. [LLW22, Corollary 4.6] says that the symplectic mapping class group of X is finite, thus $\psi^m \in \mathrm{Symp}_0(X) = \mathrm{Ham}(X)$ for some $m \geq 0$. □

3.4 Probes and displacement energy

We want to use probes to give an upper bound on the displacement energy e of a fibre of an almost toric fibration $\pi : X \to B$. Probes where introduces by McDuff in [McD11] in the context of toric symplectic manifolds. Here we consider the following slight generalisation:

Definition 3.27. Let $(B, \mathfrak{N})$ be a nodal integral affine surface. A **probe** $P : [0, d) \to B \setminus \mathfrak{N}$ is a rational straight line segment such that:

1. P intersects ∂B integrally transversely, i.e. $T_{P(0)}\partial B \cap \Lambda_{P(0)}$ and $P'(0)$ span the lattice $\Lambda_{P(0)}B$. In particular P does not intersect ∂B in a corner of B.
2. P has no self-intersections.

Note that it follows from point 1 that P' is primitive. With this definition we can choose action-coordinates on a contractible neighbourhood of P where one can perform the symplectic reduction needed for the results in [McD11]. In particular we get the following version of [Bre23, Proposition 3.4]:

Lemma 3.28. *If $P : [0, d) \to B \setminus \mathfrak{N}$ is a probe and $\pi : X \to (B, \mathfrak{N})$ is an almost toric fibration, then for $t < \frac{d}{2}$,*

$$e(\pi^{-1}(P(t))) \leq t \, .$$

Let Δ be a weakly Delzant polygonal domain. Let $(B_0, \mathfrak{N}_0)$ be the nodal integral affine surface obtained by smoothing all vertices of Δ, and $\varphi_0 : (B_0, \mathfrak{N}_0) \to \Delta$ the associated nodal chart, see Figure 3.4 a).

Theorem 3.29. *Set $M = \sup(\mathscr{F}_\Delta)$. Let $\varphi_0 : (B_0, \mathfrak{N}_0) \to \Delta$ as above, and $x \in \Delta \setminus \mathscr{K}_\Delta$ with $\mathscr{F}_\Delta(x) < \frac{1}{2}M$. Then there exists a nodal tangle $(B \times [0,1], \mathfrak{N})$ connecting $(B_0, \mathfrak{N}_0)$ to $(B_1, \mathfrak{N}_1)$ with $x \notin \varphi_0(\pi_B(\mathfrak{N}))$ and a probe $P : [0, d) \to (B_1, \mathfrak{N}_1)$ with $P(\mathscr{F}_\Delta(x)) = \varphi_1^{-1}(x)$ and $2d > \mathscr{F}_\Delta(x)$.*

Using Lemma 3.28 we immediately get the symplectic version of Theorem 3.29:

Corollary 3.30. *Let $\varphi_0 : (B_0, \mathfrak{N}_0) \to \Delta$ be as above, $x \in \Delta \setminus \mathscr{K}_\Delta$ with $\mathscr{F}_\Delta(x) < \frac{1}{2}M$, and let $\pi_0 : X \to (B_0, \mathfrak{N}_0)$ be the unique almost toric fibration over $(B_0, \mathfrak{N}_0)$.*

Then $e((\varphi_0 \circ \pi_0)^{-1}(x)) < \mathscr{F}_\Delta(x)$.

Proof of Theorem 3.29. Take $M_\varepsilon < M$ so close to M that $2\mathscr{F}_\Delta(x) < M_\varepsilon$. Let $(B \times [0,1], \mathfrak{N})$ be the nodal tangle constructed in Proposition 3.17. Since $x \notin \mathscr{K}_\Delta$, we may choose an open neighbourhood V of $\mathscr{K}_\Delta$ such that $x \in \Delta \setminus V$. By the construction of $(B \times [0,1], \mathfrak{N})$ we may assume that $\pi_B\mathfrak{N} \subset V$. Let $\pi : X \times [0,1] \to (B \times [0,1], \mathfrak{N})$ be a lift of $(B \times [0,1], \mathfrak{N})$ supported on V. In particular we have that $(\varphi_0 \circ \pi_0)^{-1}(x) = (\varphi_1 \circ \pi_1)^{-1}(x)$, where $\varphi_1 = \varphi_0 \circ \tau_1^0$.

We proceed to construct a probe P displacing $(\varphi_0 \circ \pi_0)^{-1}(x)$.

Since $x \notin \mathscr{K}_\Delta$, for small $a \in \mathbb{R}^2$ we can write $\mathscr{F}_\Delta(x + a) = \mathscr{F}_\Delta(x) + \langle \lambda, a \rangle$ for some primitive $\lambda \in \mathbb{Z}^2$. Let u be a primitive integral vector in $\Lambda_{\varphi_1^{-1}(x)} B_1$ such that

$$\partial_{D_{\varphi_1^{-1}(x)}\varphi_1(u)} \mathscr{F}_\Delta = \langle \lambda, D_{\varphi_1^{-1}(x)}\varphi_1(u) \rangle = 1 \, . \tag{3.3}$$

Here $D\varphi_1$ is well-defined at $\varphi_1^{-1}(x)$ since φ_1 is integral affine near $\varphi_1(x)$. Set $t_x = \mathscr{F}_\Delta(x)$. Take P to be the straight line with initial condition $P(t_x) = x$ and $P'(t_x) = u$. We take P to have maximal domain such that $\operatorname{im} P \subset \varphi_1^{-1}(\Delta \setminus \Delta_{M_\varepsilon})$.

Since, by Proposition 3.17, $\mathscr{F}_1$ is integral affine on $\varphi_1^{-1}(\Delta \setminus (\Delta_{M_\varepsilon} \cup \mathfrak{N}_1)) \subset (B_1, \mathfrak{N}_1)$, so is $\mathscr{F}_1 \circ P$. In particular $(\mathscr{F}_1 \circ P)'$ is constant equal to $(\mathscr{F}_1 \circ P)'(t_x) = 1$ by (3.3).

The only nodes in $\Delta \setminus \Delta_{M_\varepsilon}$ are the ones we parked near vertices of $\mathscr{K}_\Delta$ in Proposition 3.17. By performing small nodal slides at the parked nodes, we may assume that P does not hit a node. (The parked nodes slide in level sets of $\mathscr{F}_1$, in particular not parallel to the direction of P.)

Then the domain of P is $[0, M_\varepsilon)$ and $\mathscr{F}_1 \circ P = \mathrm{id}_{[0, M_\varepsilon)}$. Furthermore $(\mathscr{F}_1 \circ P)'(0) = 1$ ensures that the intersection of P and $\partial B = \mathscr{F}_1^{-1}(0)$ is integrally transverse. Since $\mathscr{F}_1 \circ P$ is injective, P has no self intersections. So P is a probe passing through $P(t_x) = \varphi_1^{-1}(x)$ with total length $M_\varepsilon > 2t_x$. □

Corollary 3.30 gives an upper bound on the displacement energy e. In case Δ is Delzant, we get a matching lower bound:

Lemma 3.31 ([Bre23, Proposition 3.4])**.** *Let $\mu : X \to \Delta$ be a toric symplectic manifold with Δ a Delzant polygonal domain. Then for all $x \in \Delta$ we have $\mathscr{F}_\Delta(x) \leq e(\mu^{-1}(x))$.*

Combining Corollary 3.30 and Lemma 3.31 we get:

Corollary 3.32. *Let $\mu : X \to \Delta$ be a toric symplectic manifold over a Delzant polygonal domain Δ. Then for all $x \in \Delta \setminus \mathscr{K}_\Delta$ with $\mathscr{F}_\Delta(x) < \frac{1}{2}\sup \mathscr{F}_\Delta$ we have $\mathscr{F}_\Delta(x) = e(\mu^{-1}(x))$.*

Remark 3.33. It may be possible to get rid of the restriction $\mathscr{F}_\Delta(x) < \frac{1}{2}\sup \mathscr{F}_\Delta$ in Theorem 3.29 and Corollary 3.32. Indeed, by continuing the straight line P in the proof of Theorem 3.29 through $\varphi_1^{-1}(\Delta_{M_\varepsilon})$, we can often get a *symmetric probe*, see [ABM14, §1.2.1], allowing us to displace all fibres of $\Delta \setminus \mathscr{K}_\Delta$ with the desired displacement energy. The challenge here is to avoid self-intersections of P. In all toric examples I examined this approach works, however I do not know a general method that always works.

4 Lagrangian knots

We summarize the procedure used to construct new Lagrangian torus knots using almost toric fibrations. This method was first used by Vianna in [Via16; Via17] to obtain monotone torus knots. The method goes as follows:

1. Create a nodal tangle $(B \times I, \mathfrak{N})$ and a lift $\pi : X \times I \to (B \times I, \mathfrak{N})$.
2. Maybe $\pi_0^{-1}(x) \ncong \pi_t^{-1}(x)$ for some $x \in B$? Use your favourite invariant to try to distinguish them.

To distinguish the monotone tori in [Via16; Via17], Vianna uses holomorphic disc counts. We will use the displacement energy germ, mostly relying on Corollary 3.32 to compute it. The displacement energy germ was first used for this purpose in [CS10].

Lemma 2.31 tells us that this approach will only work for $x \in \pi_B(\mathfrak{N})$, as other fibres are mapped to symplectomorphic fibres under nodal tangles. For fibres over $x \in \pi_B(\mathfrak{N})$, Corollary 2.34 tells us that the invariant germs of $\pi_0^{-1}(x)$ and $\pi_1^{-1}(x)$ are related by the transition map τ_0^1 created by the nodal tangle, so our goal is to create a tangle that provides a "complicated" τ_0^1 in order to change the given invariant germ.

In general, we are given $x \in B_0$ and some nodes $\mathfrak{n}_1, ..., \mathfrak{n}_n$ whose eigenlines pass through x. Then we slide some of the nodes $\mathfrak{n}_1, ..., \mathfrak{n}_n$ back and forth over x. This situation can be described by using (rank 2) cluster algebras, see for example [STW16]. To get the setup of [STW16], take straight line segments connecting x with the nodes $\mathfrak{n}_1, ..., \mathfrak{n}_n$. The *visible Lagrangians* (see e.g. [Eva23, Section 5.1]) over these straight line segments are Lagrangian discs $D_1, ..., D_n$ with boundary on $\pi^{-1}(x)$. The collection $(\pi^{-1}(x), D_1, ..., D_n)$ gives the Lagrangian skeleton of [STW16]. A *mutation* at D_i is given by a *la-disc surgery* introduced in [Yau13] and corresponds to sliding the node $\mathfrak{n}_i$ over x. See also [ABR23] for a cluster theoretic setup that can be adopted almost directly to our case. Here we take a more ad hoc approach for the cases of one or two nodes sliding over x.

4.1 Rectifying map for one node

Let $\pi_0 : X \to (B_0, \mathfrak{N}_0)$ be an almost toric fibration and let $\mathfrak{n} \in \mathfrak{N}_0$ be a node with eigenray ℓ passing through a point $x_0 \in B_0$.

Let $\varphi_0 : U \to \mathbb{R}^2$ be a nodal chart with $\{\mathfrak{n}, x_0\} \subset U$ which is integral affine near x_0, and take $(B \times I, \mathfrak{N})$ to be a nodal tangle starting at $(B_0, \mathfrak{N}_0)$ such that $\mathfrak{n}$ slides over x_0 once. Using φ_0 we identify U with $\varphi_0(U)$ for the rest of this section. Let $v \in \mathbb{Z}^2$

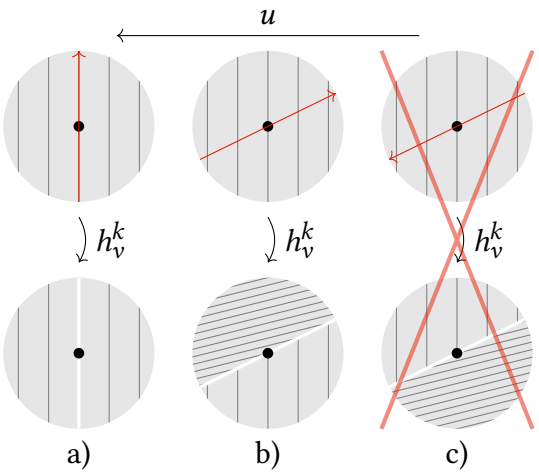

Figure 4.1: Modifying invariant germs by sliding over one node.

be the monodromy vector of $\mathfrak{n}$ and k the multiplicity of $\mathfrak{n}$. Then, using Remark 2.8, the rectifying map at $x_1 = \tau_0^1 x_0$ of $\varphi_1 = \varphi_0 \circ \tau_1^0$ is given by the half-shear h_v^k. Let $\pi : X \times I \to (B \times I, \mathfrak{N})$ be a lift of the nodal tangle. Now we may use Corollary 2.34 and Lemma 2.36 to distinguish $\pi_0^{-1}(x)$ and $\pi_1^{-1}(x)$.

Suppose we have an invariant $\mathscr{I} : \mathscr{L} \to \mathbb{R}$ which is affine near x. For example this is the case if $\mathscr{I}$ is the displacement energy and we are in the setting of Corollary 3.32 with x not being in the caustic.

Using Lemma 2.36 we may identify the invariant germ $[\mathscr{I}]_{\pi_0^{-1}(x_0)}$ with $[\mathscr{I}]_{x_0}$, and similarly for x_1. Using Corollary 2.34 we can write $[\mathscr{I}]_{x_1}|_{U\setminus\ell} = [\mathscr{I}]_{x_0}|_{U\setminus\ell} \circ h_v^k$, where we have used that the rectifying map of φ_1 at x_1 is given by h_v^k.

Since $\mathscr{I}$ is linear near x_0, there is $u \in \mathbb{R}^2$ such that $\mathscr{I}(a) = \langle u, a\rangle$ for $a \in U$ near x_0. We distinguish the following cases, illustrated in Figure 4.1:

a) If $\langle u, v\rangle = 0$ then $[\mathscr{I}]_{x_1}|_{U\setminus\ell} = [\mathscr{I}]_{x_0}|_{U\setminus\ell} \circ h_v^k = [\mathscr{I}]_{x_0}|_{U\setminus\ell}$, so $\pi_0^{-1}(x)$ cannot be distinguished from $\pi_1^{-1}(x)$ using Corollary 2.34.
b) If $\langle u, v\rangle < 0$, then the germs $[\mathscr{I}]_{x_1}|_{U\setminus\ell} = [\mathscr{I}]_{x_0}|_{U\setminus\ell} \circ h_v^k$ and $[\mathscr{I}]_{x_0}$ are not related by an integral linear transformation, so $\pi_0^{-1}(x)$ and $\pi_1^{-1}(x)$ are not related by symplectomorphism. Let $p = -\langle u, v\rangle, q = \det(u, v)$. Then the invariant germ of $\pi_1^{-1}(x)$ is the same (away from ℓ) as the displacement energy germ of the torus $T_{pq}^k(\mathscr{I}(x))$ constructed in [BHS24].
c) We think that $\langle u, v\rangle > 0$ never happens (at least when $\mathscr{I}$ is the displacement energy), as it would lead to an invariant germ which does not look like a tropical polynomial, see [Bre25, Question 5.4 and Remark 2.18].

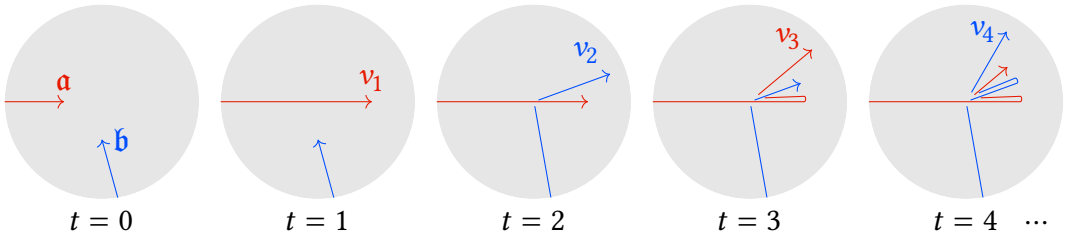

Figure 4.2: Entangling two nodes

4.2 Entangling nodes: Rectifying maps for two nodes

Let $\pi_0 : X \to (B_0, \mathfrak{N}_0)$ be an almost toric fibration and $\mathfrak{a}, \mathfrak{b} \in \mathfrak{N}_0$ two nodes. Assume that the eigenlines γ_0, γ_1 of $\mathfrak{a}$ and $\mathfrak{b}$ respectively have some intersection point $x \in B$. Modifying B_0 by a nodal tangle if necessary, we may assume that $\mathfrak{a}$ and $\mathfrak{b}$ are contained in a small contractible neighbourhood U_0 of x containing no other nodes.

We want to study the nodal tangle obtained by alternatingly sliding $\mathfrak{a}$ and $\mathfrak{b}$ through x. We define it recursively: For $n \in 2\mathbb{Z}_{\geq 0}$, let $(B_{n+1}, \mathfrak{N}_{n+1})$ be the nodal integral affine surface obtained from $(B_n, \mathfrak{N}_n)$ by sliding $\mathfrak{a}$ through x once, and let $(B_{n+2}, \mathfrak{N}_{n+2})$ be the nodal integral affine surface obtained from $(B_{n+1}, \mathfrak{N}_{n+1})$ by sliding $\mathfrak{b}$ through x once. We obtain a nodal tangle $(B \times \mathbb{R}_{\geq 0}, \mathfrak{N})$. See Figure 4.2.

Let $\varphi_0 : U \to \mathbb{R}^2$ be an integral affine chart of $(B_0, \mathfrak{N}_0)$ at x. Then $\varphi_t = \varphi_0 \circ \tau_0^t$ is a nodal chart of $(B_t, \mathfrak{N}_t)$ for all $t \geq 0$. For the rest of the discussion, identify U with its image $\varphi_t(U) \subset \mathbb{R}^2$.

For $n \in \mathbb{Z}_{\geq 0}$ odd let v_n be the primitive vector such that at time $t = n$ the node $\mathfrak{a}$ lies on the ray in direction v_n emanating from x. For $n \in \mathbb{Z}_{\geq 0}$ even let v_n be the primitive vector such that at time $t = n$ the node $\mathfrak{b}$ lies on the ray in direction v_n emanating from x. In both cases v_n coincides with the monodromy vector field of $\mathfrak{a}$ resp. $\mathfrak{b}$ near $\mathfrak{a}$ resp. $\mathfrak{b}$ at time $t = n$.

For times t where $x \notin \mathfrak{N}_t$, denote by R_t a choice of rectifying map of φ_t at x, so that $R_t \circ \varphi_t$ is an integral affine chart of $(B_t, \mathfrak{N}_t)$ at x. From Figure 4.2 and Remark 2.8 we see that R_1 is given by the half-shear $h_\mathfrak{a} := h_{v_1}^{k_\mathfrak{a}}$, and R_2 is given by the composition of half-shears $h_\mathfrak{b} \circ h_\mathfrak{a}$, where $h_\mathfrak{b} := h_{-v_0}^{k_\mathfrak{b}}$. Set

$$R = -\operatorname{id} \circ R_2 = -h_\mathfrak{b} \circ h_\mathfrak{a},$$

which is another choice of rectifying map of φ_2 at x. Note that the nodes $\mathfrak{a}, \mathfrak{b}$ at time $t = 0$ are on the rays given by the pair $(-v_1, v_0)$, and for time $t = 2$ they are on the rays v_1 and $v_2 = -v_0 + k_\mathfrak{a} \det(v_0, v_1) v_1$, where we used Remark 2.19 to calculate v_2. We quickly check that $Rv_1 = -v_1$ and $Rv_2 = v_0$, so the images of φ_0 and $R\varphi_2$ are identical. Iterating, we can write the other rectifying maps as $R_{2n} = (-R)^n = (h_\mathfrak{b} \circ h_\mathfrak{a})^n$ and

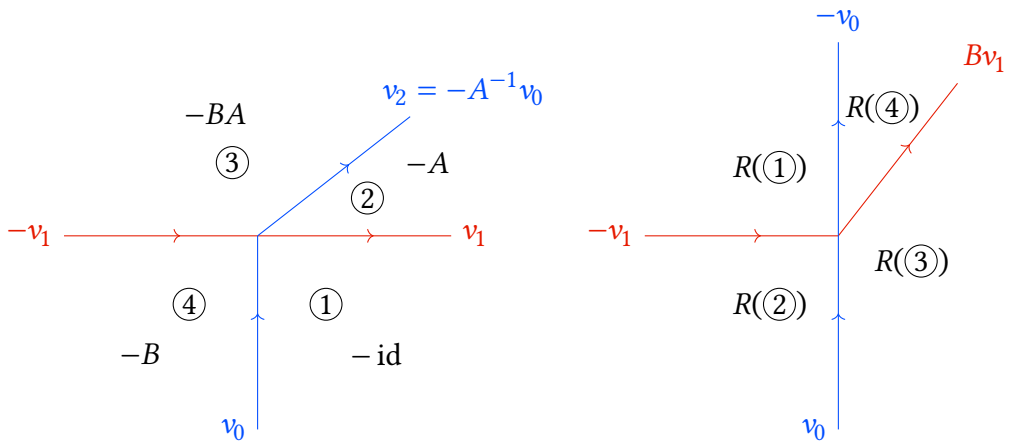

Figure 4.3: The rectifying map R. On the left the domain of R and on the right its image. The domain is divided into four closed cones ①, ②, ③, ④ on which R acts linearly by the matrices $-\mathrm{id}, -A, -BA, -B$ respectively. The rays dividing these regions form the cut graph of R (and of R^{-1} on the right), and are labelled by the corresponding orientation.

$R_{2n+1} = h_{\mathfrak{a}} \circ R_{2n} = h_{\mathfrak{a}} \circ (h_{\mathfrak{b}} \circ h_{\mathfrak{a}})^n$. We also get an explicit formula for v_n:

$$\begin{aligned} v_{2n-1} &= R^{-n}(-v_1) \\ v_{2n} &= R^{-n}(v_0) \end{aligned} \tag{4.1}$$

Set $a = \det(v_0, v_1)k_{\mathfrak{a}}, b = \det(v_0, v_1)k_{\mathfrak{b}}$ and take $(v_1, -v_0)$ as basis of $\mathbb{R}^2$. In this basis the piecewise linear map R can be written as in Figure 4.3, where

$$A := s_{v_1}^{k_{\mathfrak{a}}} = \begin{pmatrix} 1 & -a \\ 0 & 1 \end{pmatrix}, \quad B := s_{v_0}^{k_{\mathfrak{b}}} = \begin{pmatrix} 1 & 0 \\ b & 1 \end{pmatrix}.$$

The following proposition says when we can expect "interesting" rectifying maps. Recall that $a, b \in \mathbb{Z}_{\geq 1}$.

Proposition 4.1. *We have*

- *If $ab = 1$ then R_n is linear iff $n \in 5\mathbb{Z}_{\geq 0}$.*
- *If $ab = 2$ then R_n is linear iff $n \in 6\mathbb{Z}_{\geq 0}$.*
- *If $ab = 3$ then R_n is linear iff $n \in 8\mathbb{Z}_{\geq 0}$.*
- *If $ab \geq 4$ then R_n is not linear for any $n > 0$. The rectifying map $R_{2n} = (-1)^n R^n$ can be written as in Figure 4.5, and we may write*

$$\begin{aligned} v_{2n-1} &= bv_{2n-2} - v_{2n-3} = (-BA)^{1-n} v_1 \\ v_{2n} &= av_{2n-1} - v_{2n-2} = (-BA)^{1-n} v_2 \,. \end{aligned} \tag{4.2}$$

The proof will require some preparations.

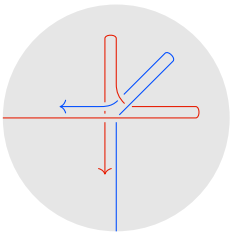

Figure 4.4: Nodal tangle diagram for the case $ab = 1$ at $t = 5$. Here the rectifying map at x is integral linear.

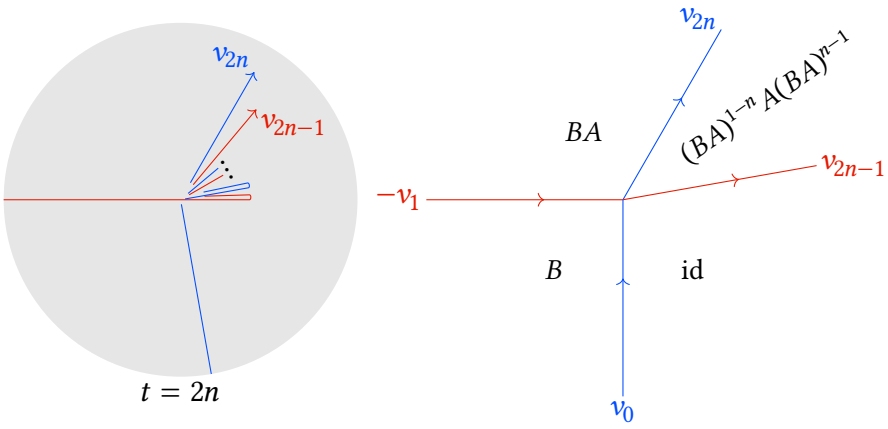

Figure 4.5: The rectifying map R_{2n}

Remark 4.2. The cases $ab = 1, 2, 3$ appear in [CV21, Section 3.2], where they are related to A_2, B_2, G_2 cluster relations.

This is a general phenomenon: Using the setup of [ABR23], we see that a cluster relation corresponds to a local nodal braid, that is a nodal tangle near x such that $(U_0, \mathfrak{N}_0) = (U_1, \mathfrak{N}_1)$. The nodal braid for $ab = 1$ is illustrated in Figure 4.4.

Remark 4.3. In the last case of Proposition 4.1, if $a = b \geq 2$ then the recurrence relation in (4.2) is a linear recurrence relation with constant coefficients:

$$v_n = av_{n-1} - v_{n-2} \,. \tag{4.3}$$

By the using e.g. generating functions we can thus find a closed form for v_n: Let $\mu^{\pm 1} = \frac{a \pm \sqrt{a^2-4}}{2}$ be the solutions to the characteristic polynomial of (4.3). Then we have

$$v_n = \begin{cases} v_0 + n(v_1 - v_0) & \text{if } a = 2 \\ \frac{1}{\sqrt{a^2-4}}\left((\mu^n - \mu^{-n})v_1 - (\mu^{n-1} - \mu^{1-n})v_0\right) & \text{if } a > 2 \end{cases} .$$

To prove Proposition 4.1 we use the following definition and lemma.

Definition 4.4. A vector $u \neq 0$ is an **eigenvector** of a piecewise linear map T if

$$Tu = \lambda u$$

for some **eigenvalue** $\lambda \in \mathbb{R}_{>0}$.

Lemma 4.5. *Let C be the cone $③ \cap R(③)$.*

- *If $ab < 4$ then R has no eigenvector,*
- *if $ab = 4$ then R has exactly one eigenvector, which is contained in C,*
- *if $ab > 4$ then R has exactly two eigenvectors, which are contained in C.*

Proof. By definition, we have $C \subset ③$. We see from Figure 4.3 that

$$\begin{aligned} R(①) &\subset ③ & R(②) &= ④ \\ R(③) &\subset ① \cup ② \cup ③ & R(④) &\subset ③\,, \end{aligned}$$

so ③ is the only region which may intersect its image under R, and there cannot be any eigenvectors in the regions ①, ②, ④. Since $R|_{③} = -BA$, if R has eigenvectors in ③ then they are also eigenvectors of the integral linear map $-BA$.

In the basis $(v_1, -v_0)$, we can write $-BA$ as the matrix

$$\begin{pmatrix} -1 & a \\ -b & ab-1 \end{pmatrix}.$$

The discriminant of the characteristic polynomial of $-BA$ is $ab(ab-4)$, showing that $-BA$ has the desired number of eigenvectors. We claim they are contained in C if they exist.

Let $ab \geq 4$. Calculating the eigenvalues and eigenvectors, we get

$$\lambda^{\pm 1} = \frac{ab - 2 \pm \sqrt{ab(ab-4)}}{2}, \quad u_{\lambda^{\pm 1}} = \begin{pmatrix} ab \mp \sqrt{ab(ab-4)} \\ 2b \end{pmatrix}$$

and using $\det(-BA) = 1$ we get $\lambda > 1 > \lambda^{-1} > 0$.

The cone C is spanned by $(v_2, Bv_1) = ((a,1),(1,b))$. We can write

$$(ab-1)u_{\lambda^{\pm 1}} = 2b\lambda^{\mp 1}v_2 + 2(\lambda^{\pm 1} + 1)Bv_1$$

where the coefficients $2b\lambda^{\mp 1}$ and $2(\lambda^{\pm 1} + 1)$ are both positive, so $u_{\lambda^{\pm 1}}$ is indeed contained in C. □

Proof of Proposition 4.1. The cases $ab = 1, 2, 3$ are straightforward to check by hand using the fact that $ab = 1, 2, 3$ implies that $\det(v_0, v_1) = 1$ and $\{k_{\mathfrak{a}}, k_{\mathfrak{b}}\} = \{a, b\} = \{1, ab\}$. The case $ab = 1$ is illustrated in Figure 4.4.

So let $ab \geq 4$. Then by Lemma 4.5, R^n has at least one eigenvector, and all of its eigenvectors are contained in the cone C. This means R^n is not linear: If R^n was

linear, it would also have at least one eigenvector in the cone $-C$. Thus $R_{2n} = (-R)^n$ is also not linear. The cuts of R_{2n+1} are given by the rays spanned by the vectors $-v_1, v_0, v_{2n}, v_{2n+1}$. Below we will see that these are all distinct, and thus R_{2n+1} is also not linear.

By (4.1),

$$\begin{aligned} v_{2n-1} &= R^{-n}(-v_1) = R^{1-n}(v_1) \\ v_{2n} &= R^{-n}(v_0) \quad = R^{1-n}(v_2)\,. \end{aligned}$$

The pair v_1, v_2 is contained in the positive cone $\langle v_0, u_{\lambda^{-1}}\rangle_+$ spanned by $v_0, u_{\lambda^{-1}}$, with $u_{\lambda^{-1}}$ as in the proof of Lemma 4.5. (This follows from the fact that $u_{\lambda^{-1}}$ is contained in C which is spanned by (v_2, Bv_1).) On $\langle v_0, u_{\lambda^{-1}}\rangle_+ \subset R(③)$ the map R^{-1} is given by $(-BA)^{-1}$. Under repeated iterations of R^{-1}, $u_{\lambda^{-1}}$ is the attractive eigenvector of $(-BA)^{-1}$, meaning that the sequence $\frac{v_n}{|v_n|}$ in S^1 converges monotonically to $\frac{u_{\lambda^{-1}}}{|u_{\lambda^{-1}}|}$, so that v_n is contained in $\langle v_0, u_{\lambda^{-1}}\rangle_+$ for all $n \geq 1$. This lets us give an explicit formula for the v_n:

$$\begin{aligned} v_{2n-1} &= (-BA)^{1-n} v_1 \\ v_{2n} &= (-BA)^{1-n} v_2\,, \end{aligned}$$

from which we easily deduce the recurrence

$$\begin{aligned} v_{2n-1} &= -v_{2n-3} + b v_{2n-2} \\ v_{2n} &= -v_{2n-2} + a v_{2n-1}\,. \end{aligned}$$

The cones where R_{2n} is linear are given by the vectors $-v_1, v_0, v_{2n-1}, v_{2n}$ as indicated in Figure 4.5. Using Figure 4.3, we see that in the lower right cone $\langle v_0, v_{2n-1}\rangle_+$ the map $R_{2n} = (-R)^n$ is given by the identity.

Note that shear maps transform under linear bijections like

$$s_{Tv} = T s_v T^{-1}\,.$$

Now we can use this identity and Remark 2.8 to determine the map R_{2n} on the remaining cones: The ray given by $v_{2n-1} = (-BA)^{1-n} v_1$ is a cut of weight $k_{\mathfrak{a}}$, and the associated shear map is given by

$$\begin{aligned} s^{k_{\mathfrak{a}}}_{(-BA)^{1-n}v_1} &= (-BA)^{1-n} s^{k_{\mathfrak{a}}}_{v_1} (-BA)^{n-1} \\ &= (-BA)^{1-n} A (-BA)^{n-1} = (BA)^{1-n} A (BA)^{n-1}\,. \end{aligned}$$

The linear maps on the two other cones are determined similarly. Similarly we can also determine the rectifying map for R_{2n+1}. □

The following theorem describes a situation where we get an infinite family of Lagrangian tori which are not Hamiltonian isotopic, see Figure 1.4.

Theorem 4.6. *Let $\pi : X \to (B_0, \mathfrak{N}_0)$ be an almost toric fibration, and $x_0 \in B_0$. Suppose that*

1. *There are two nodes $\mathfrak{a}, \mathfrak{b}$ incident at x_0 with*

$$k_\mathfrak{a} k_\mathfrak{b} \det(v_\mathfrak{a}, v_\mathfrak{b})^2 \geq 4$$

   where $k_\mathfrak{a}, k_\mathfrak{b}$ are the multiplicities of $\mathfrak{a}$ and $\mathfrak{b}$ and $v_\mathfrak{a}, v_\mathfrak{b}$ are the monodromy vector fields of $\mathfrak{a}$ and $\mathfrak{b}$.
2. *$\mathcal{I} : \mathcal{L} \to \mathbb{R}$ is an invariant of Lagrangians under symplectomorphisms such that the invariant germ $[\mathcal{I}]_{x_0} : B_0 \to \mathbb{R}$ is affine and non-constant on an open dense set near x_0.*

Let $(B \times \mathbb{R}_{\geq 0})$ be the nodal tangle obtained as above by sliding $\mathfrak{a}$ and $\mathfrak{b}$ alternatingly over x.

Then the invariant germs $[\mathcal{I}]_{x_0} \circ \tau_n^0$ are pairwise different, hence the Lagrangian tori $\{\pi_n^{-1}(x)\}$ are pairwise not related by symplectomorphism.

Proof. Condition 1. puts us in the case $ab \geq 4$ in Proposition 4.1.

Let φ_0 be an integral affine chart at x_0, and let $\varphi_n := \varphi_0 \circ \tau_n^0$ and $x_t = \tau_0^t x_0$. An integral affine chart at x_n is given by $R_n \circ \varphi_n$, where R_n is the rectifying map of φ_n at x_n. Identifying a neighbourhood of x_n with its image under $R_n \circ \varphi_n$, the invariant germ $[\mathcal{I}]_{x_0} \circ \tau_n^0$ is given by $[\mathcal{I}]_{x_0} \circ R_n$.

Since $[\mathcal{I}]_{x_0}$ is affine, the cut graph of $[\mathcal{I}]_{x_0} \circ R_n$ is the same as the one of R_n, except for possibly one edge missing. The cut graph of R_n is given by the rays spanned by the vectors $-v_1, v_0, v_{n-1}, v_n$, see Figure 4.5 for the case where n is even. The cut graphs of R_n are all not related by an integral affine transformation by Equation (4.2), and removing one edge does not change that. By Lemma 2.36 this suffices to show that the Lagrangian tori $\pi_n^{-1}(x_n)$ are not related by symplectomorphism. □

4.3 Examples

Example 4.7 ($S^2 \times S^2$)**.** Take $S^2 \times S^2$ with the symplectic form $\omega_\alpha = 2(1+\alpha)\omega_{S^2} \oplus 2\alpha\omega_{S^2}$ where $\alpha > 0$, and let $\square_\alpha = [-(1+\alpha), 1+\alpha] \times [-\alpha, \alpha] \subset \mathbb{R}^2$ be the moment image under the usual Hamiltonian torus action $\mu : (S^2 \times S^2, \omega_\alpha) \to \square_\alpha$. This normalization corresponds to the one chosen in [BK25]. It means that the caustic $\mathscr{K}_{\square_\alpha}$ is independent of α.

After nodal trades at the corners of $\square_\alpha$, the points $(-1, 0), (1, 0)$ both lie on the intersection of eigenlines of nodes as in Section 4.2, see Figure 4.6. With the notation of Proposition 4.1, at $x = (-1, 0)$ we have two incoming nodes $\mathfrak{a}, \mathfrak{b}$ with $a = b = 2$ and $v_0 = (-1, 1), v_1 = (1, 1)$. Entangling these nodes at x, we see from Remark 4.3 that we can get nodes exiting x in the directions $(2n+1, 1)$ for $n \geq 0$. Swapping the roles of $\mathfrak{a}, \mathfrak{b}$ (i.e. sliding $\mathfrak{b}$ over x first, resulting in setting $v_0 = (-1, -1), v_1 = (1, -1)$) we also get nodes exiting x in the directions $(2n+1, -1)$. Similarly, we can get nodes exiting $(1, 0)$ in the directions $(-(2n+1), \pm 1)$ for $n \geq 0$.

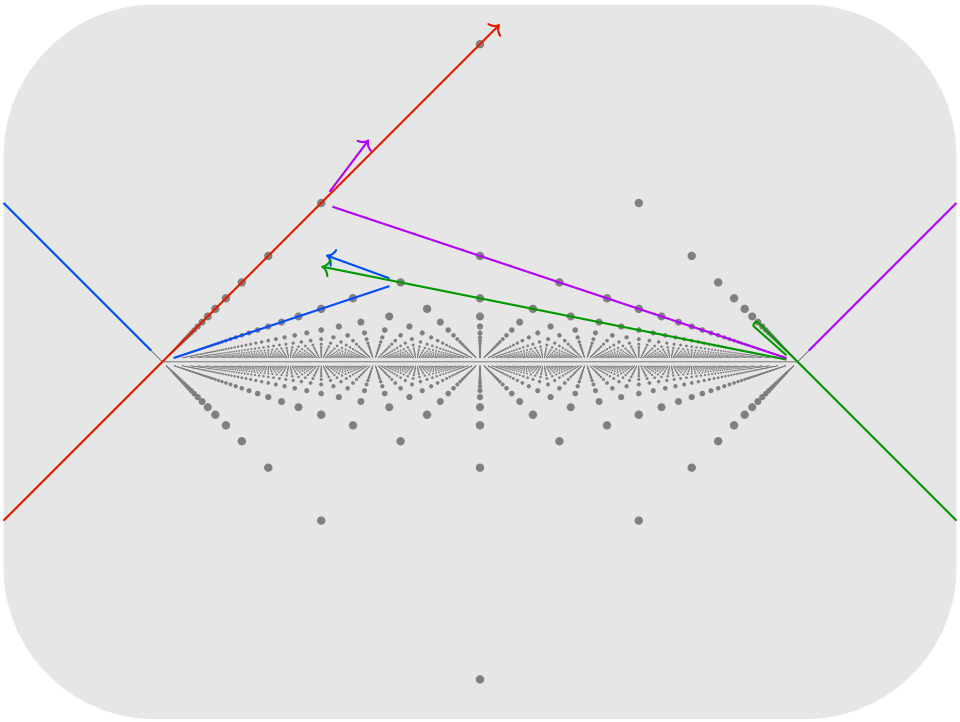

Figure 4.6: Some Lagrangian knots in $S^2 \times S^2$; we only picture the interior of the moment polytope. Grey dots correspond to points in $\mathscr{D}'$.

Eigenrays of these nodes may again intersect in one of the points of

$$\mathscr{D}' = \left\{ \left(\frac{k-2l-1}{k}, \pm\frac{1}{k} \right) \,\middle|\, k \in \mathbb{Z}_{\geq 1}, l \in \{0, \ldots, k-1\} \right\}.$$

Over these points, entangling two nodes gives infinitely many Lagrangian torus knots. The displacement energy germs of two families over two points in $\mathscr{D}'$ have the same displacement energy germs if and only if their y-coordinate is the same. (This means that in $\mathscr{D}'$ they share the same value of k, and we have that $a = 2k$ in Remark 4.3, resulting in the same displacement energy germs.)

Of course there are many other points in $\square_\alpha$ where we can entangle two nodes, which are however more difficult to determine.

The set $\mathscr{D}'$ coincides with the set of toric fibres which are not *ball non-monotone*, see [BK25, Theorem 1.23].

Note that at $(\pm 1, 0)$ entangling the nodes has no effect on the displacement energy germ. Indeed, using probes it can be shown that all tori constructed by entangling at $(\pm 1, 0)$ are Hamiltonian isotopic.

Example 4.8 (Vianna Tori). A **Markov triple** $(p_1, p_2, p_3) \in \mathbb{N}^3$ is a triple satisfying the Markov equation

$$p_1^2 + p_2^2 + p_3^2 = 3p_1p_2p_3 \,.$$

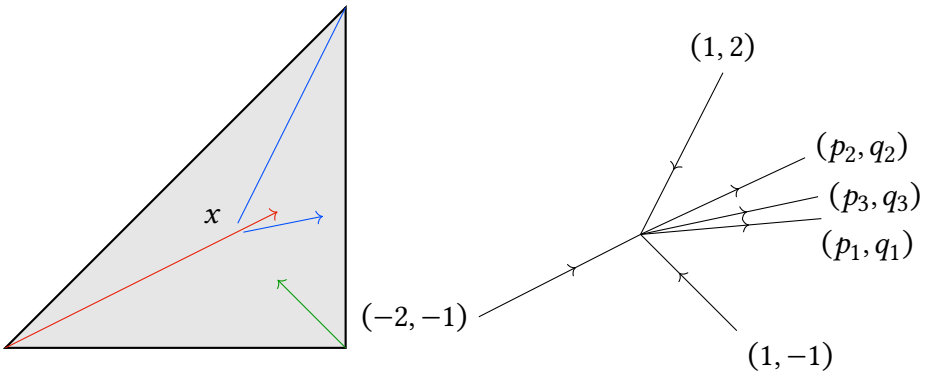

a) The Vianna torus $T_{1,2,5}$

b) Rectifying map for a Markov triple (p_1, p_2, p_3)

Figure 4.7: Constructing Vianna tori via nodal tangles

In [Via16], Vianna constructed a monotone Lagrangian knot in $\mathbb{C}P^2$ for every Markov triple by following the outline given at the start of Chapter 4. Denote by T_{p_1,p_2,p_3} Vianna's torus corresponding to the Markov triple p_1, p_2, p_3. See [Eva23, Appendix I] for a nice exposition on the connection between the base diagrams and the Markov equation. We do not give a full description of the construction, but just describe the rectifying map obtained by following Vianna's sequence of nodal slides starting from the standard toric base diagram for $\mathbb{C}P^2$ and interpreting it as a nodal tangle.

In Figure 4.7 a), the fibre over the central point x is the torus $T_{5,2,1}$. Realize a sequence of mutations to arrive at the Markov triple (p_1, p_2, p_3) as a nodal tangle as done by Vianna and denote by φ_1 the corresponding nodal chart. We arrive at a situation where the rectifying map at x of φ_1 is given as in Figure 4.7 b) where (p_i, q_i) form an "extended Markov triple", including the q_i described in [ES18]. Concretely, $p = (p_1, p_2, -p_3)$ and $q = (q_1, q_2, -q_3)$ satisfy the equation

$$p \times q = 3(p_1, p_2, \hat{p}_3)\,, \tag{4.4}$$

where $\hat{p}_3 = 3p_1p_2 - p_3$ is the Markov number given by mutation at p_3. This equation follows from the fact that $\frac{1}{p_1}(p_1, q_1)$, $\frac{1}{p_2}(p_2, q_2)$, $\frac{1}{\hat{p}_3}(-p_3, -q_3)$ form the corners of a *Vianna triangle*, see [Eva23, Appendix I] for details, especially [Eva23, Corollary I.13]. The Markov equation for (p_1, p_2, p_3) follows also from (4.4).

In $\mathbb{C}P^2$, the displacement energy of toric fibres is given by $\mathscr{F}_\Delta$, except for the central fibre at x, which is non-displaceable. Applying the rectifying map R_x of φ_1, as pictured in Figure 4.7 b), the level sets of $\mathscr{F}_\Delta \circ R_x^{-1}$ give smaller copies of the Vianna triangle with corners $\frac{1}{p_1}(p_1, q_1)$, $\frac{1}{p_2}(p_2, q_2)$, $\frac{1}{\hat{p}_3}(-p_3, -q_3)$, which allows us to distinguish the Vianna tori using the displacement energy germ.

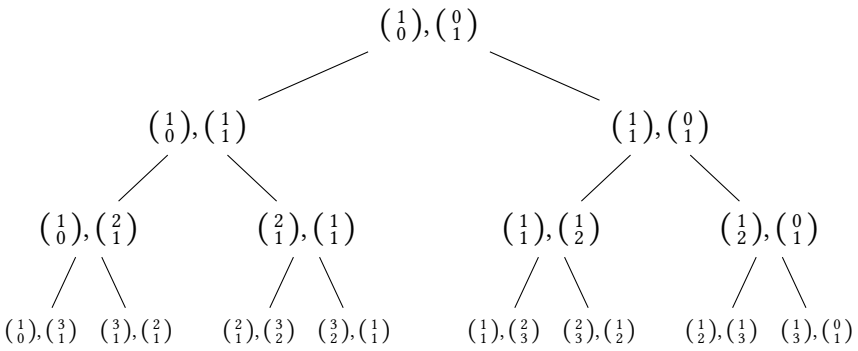

Figure 4.8: The first four rows of the Farey tree.

Example 4.9 (Farey tree & Lagrangian Pinwheels)**.** Let $\mathfrak{a} \in \mathfrak{N}$ be a node of a nodal integral affine surface, and let γ be an eigenray of $\mathfrak{a}$ intersecting ∂B in x. Near x, let u be a primitive vector parallel to ∂B and extend the monodromy pair (v, λ) of $\mathfrak{a}$ along γ to x. The *visible Lagrangian* over γ (see [Eva23, Chapter 5]) is the *Lagrangian pinwheel* $L_{p,q}$ (see [ES18, Definition 2.1]), where $p = |\det(u, v)|$ and $q = \langle u, v \rangle \mod p$. Here the scalar product is defined by some choice of basis of $\Lambda_x B$, thus q is only well-defined up to sign (since we don't fix an orientation of B).

In [ES18] it is shown that $\mathbb{C}P^2$ does only allow embeddings for certain pinwheels, namely if p is a Markov number.

Alternatively, Lagrangian pinwheels may be obtained as the vanishing cycles of a $\mathbb{Q}$-Gorenstein smoothing of a Wahl singularity. For a del Pezzo surface X, in the recent [UZ25] it is shown which Wahl singularities arise from degenerations of X, meaning which Lagrangian pinwheels can be realized "algebraically". In particular [UZ25, Theorem 1.10] states that for $X = \mathbb{C}P^2 \# n\overline{\mathbb{C}P^2}$ with $n \geq 5$ all Lagrangian pinwheels $L_{p,q}$ admit embeddings into X.

The Farey tree is a well-known procedure to generate all primitive vectors in the positive quadrant of $\mathbb{Z}^2$:

Definition 4.10. A **Farey pair** (v_0, v_1) is a positive basis of $\mathbb{Z}^2$, i.e. $\det(v_0, v_1) = 1$. Its children are the Farey pairs $(v_0, v_0 + v_1)$ and $(v_0 + v_1, v_1)$.

The **Farey tree** is the binary tree of Farey pairs with root $\left(\binom{1}{0}, \binom{0}{1}\right)$. See Figure 4.8.

Reading the n-th row of the tree from left to right ignoring repeated entries, the vectors encode the numerator and denominator of the fractions in the *Farey sequence* F_n.

Suppose that B is a nodal integral affine surface, $x \in B$ with three incoming nodes $\mathfrak{a}_1, \mathfrak{a}_2, \mathfrak{a}_3$ of multiplicity 2 on the rays originating from x spanned by primitive vectors v_1, v_2, v_3 such that $\det(v_1, v_2) = \det(v_2, v_3) = \det(v_3, v_1) = 1$. This means that x admits a nodal chart diagram as in Figure 4.9 a). Then $v_1 + v_2 + v_3 = 0$.

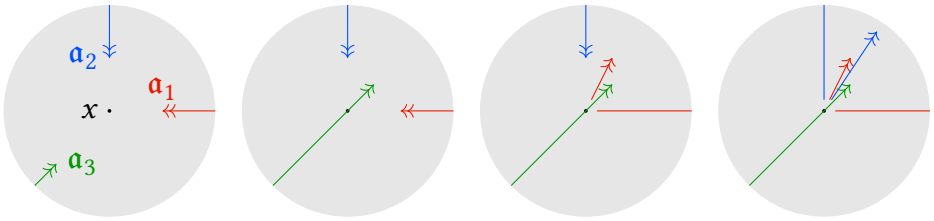

Figure 4.9: Stepping through the Farey tree with nodal slides. The double arrow heads mark that the nodes are of multiplicity two.

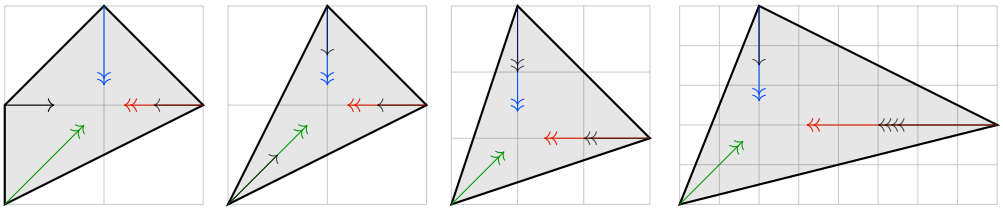

Figure 4.10: Nodal chart diagrams for monotone $\mathbb{C}P^2\#n\overline{\mathbb{C}P^2}$ with $n \geq 5$ showing the desired nodal configuration.

Pushing node $\mathfrak{a}_3$ through x, we get nodes on the rays $(v_1, v_1 + v_2, v_2)$, see Figure 4.9 b). Note that the outer vectors (v_1, v_2) form a Farey pair. Pushing one of the "outer nodes" on v_1 or v_2 through x by using the recipe in Remark 2.19, we get nodes either on the rays $(v_1 + v_2, (v_1 + v_2) + v_2, v_2)$ or $(v_1, v_1 + (v_1 + v_2), v_1 + v_2)$, with the outer vectors corresponding to the children of the Farey pair (v_1, v_2). Iterating, we see that we can reconstruct the Farey tree through nodal tangles at x.

In particular, for any primitive vector $v \in \Lambda_x B$, there exists a nodal tangle at x such that a node of multiplicity 2 slides along the ray spanned by v.

This configuration of nodes can be found in the monotone $\mathbb{C}P^2\#n\overline{\mathbb{C}P^2}$ with $n \geq 5$, as illustrated in Figure 4.10, see [Via17, Section 3] for a construction of these diagrams. In each case we can quickly check that for each primitive vector (p, q), we can find a $L_{p,q}$ pinwheel: Take a nodal chart φ as in Remark 3.18. The nodal tangles constructed above allow us to slide a node of multiplicity two along any primitive vector v pointing from x to the boundary. In the nodal chart φ we can directly read off the type of pinwheel from the coordinates of $v = (v_1, v_2)$ in φ:

$$p = |\det(v, (1, 0))| = |v_2|\,, \quad q = \langle v, (1, 0)\rangle \mod p = v_1 \mod p\,.$$

Since any primitive vector v can be realized by a nodal tangle as described above, we can find Lagrangian pinwheel $L_{p,q}$ for any coprime p, q.

5 Some open questions

5.1 The piecewise integral linear group

In this paper all piecewise integral linear transformations we encountered were generated by half-shears.

Question 5.1. Is the group of piecewise (integral) linear automorphisms of $\mathbb{R}^2$ generated by half-shears?

Remark 5.2. The answer for this question in dimensions higher than two is false. Take for example the piecewise integral linear automorphism

$$T : \mathbb{R}^3 \to \mathbb{R}^3$$
$$(x, y, z) \mapsto \begin{cases} (x, y, z) & \text{if } x \leq 0, y \leq 0 \\ (x, y, z + x) & \text{if } x \geq 0, x \geq y \\ (x, y, z + y) & \text{if } y \geq 0, y \geq x \end{cases}.$$

Indeed, if T was a composition of half-shears, it would have an even number of linear domains.

5.2 Generalizing Symington's conjecture

Consider the set $\mathscr{B}_X$ of nodal integral affine surfaces that arise as almost toric bases of a symplectic four manifold X. Extending the definition of nodal tangle to include nodal trades, Theorem A says that if X is toric, any two Delzant polygons $\Delta_0, \Delta_1 \in \mathscr{B}_X$ are connected by a nodal tangle.

Question 5.3. If X is toric, are any two nodal integral affine surfaces in $\mathscr{B}_X$ related by a nodal tangle?

Note that there might be an almost toric base of X which is not connected to a toric base by a nodal tangle.

We ask a stronger question:

Question 5.4. If X is a symplectic rational surface, are any two nodal integral affine surfaces in $\mathscr{B}_X$ related by a nodal tangle?

For both these questions it might be possible to generalize the proof strategy of Theorem A, namely trying to deform elements of $\mathscr{B}_X$ into a canonical form which only depends on X.

Being a symplectic rational surface exactly means that all bases in $\mathscr{B}_X$ are topologically discs with marked points. This follows from [LS10, Table 1], which classifies the closed symplectic 4-manifolds X that admit an almost toric fibration and their bases up to diffeomorphism. We can also ask the same question for the other types of X appearing in the list given in [LS10]:

Question 5.5. If X is a closed symplectic four manifold admitting an almost toric fibration, are any two nodal integral affine surfaces in $\mathscr{B}_X$ related by a nodal tangle?

5.3 Displacement energy of (almost) toric fibres

Question 5.6. If Δ is a Delzant polygonal domain, is the displacement energy of toric fibres given by $\mathscr{F}_\Delta$ for all points outside the caustic $\mathscr{K}_\Delta$?

See also Remark 3.33.

5.4 Tangling points

To apply our recipe for constructing Lagrangian knots, we need to find a point $x \in B$ where, perhaps after modifying B by a nodal slide, at least two eigenlines of nodes intersect.

Question 5.7. Given a nodal integral affine surface $(B, \mathfrak{N})$, what are its "entangling points" $\mathscr{D}$ where we can entangle two (or more) nodes as in Section 4.2? What are the accumulation points of $\mathscr{D} \subset B$? Can $\mathscr{D}$ be dense in a non-empty open subset of B?

These seem to be very hard combinatorial questions. An accumulation point x of $\mathscr{D}$ gives a fibre where there are infinitely many families of almost Hamiltonian isotopic Lagrangian knots nearby (in terms of Lagrangian flux). The simplest case is for monotone polygonal domains Δ such as in Examples 4.8 and 4.9, where $\mathscr{D}$ contains only the central point. In the simplest non-monotone example, Example 4.7, we already have an infinite subset $\mathscr{D}' \subset \mathscr{D}$, which has Δ_M as accumulation points.

Bibliography

[ABM14] Miguel Abreu, Matthew Strom Borman, and Dusa McDuff. "Displacing Lagrangian toric fibers by extended probes". *Algebr. Geom. Topol.* 14.2 (2014), pp. 687–752. DOI: 10.2140/agt.2014.14.687.

[ABR23] Peter Albers, Maria Bertozzi, and Markus Reineke. *Floer potentials, cluster algebras and quiver representations*. Preprint, arXiv:2309.16009. 2023.

[BHS24] Joé Brendel, Johannes Hauber, and Joel Schmitz. *Semi-Local Exotic Lagrangian Tori in Dimension Four*. Preprint, arXiv:2403.00408. To appear in Annales de l'Institut Fourier. 2024.

[BK25] Joé Brendel and Joontae Kim. *Lagrangian split tori in $S^2\times S^2$ and billiards*. Preprint, arXiv:2502.03324. To appear in Selecta Mathematica. 2025.

[Bre23] Joé Brendel. "Real Lagrangian tori and versal deformations". *J. Symplectic Geom.* 21.3 (2023), pp. 463–507. DOI: 10.4310/JSG.2023.v21.n3.a2.

[Bre25] Joé Brendel. "Local exotic tori". *Trans. Am. Math. Soc.* 378.6 (2025), pp. 4369–4411. DOI: 10.1090/tran/9385.

[BS14] Erwan Brugallé and Kristin Shaw. "A bit of tropical geometry". *Am. Math. Mon.* 121.7 (2014), pp. 563–589. DOI: 10.4169/amer.math.monthly.121.07.563.

[BS24] Filip Brocić and Egor Shelukhin. *A counterexample to Lagrangian Poincaré recurrence*. Preprint, arXiv:2409.14225. 2024.

[Che96] Yu. V. Chekanov. "Lagrangian tori in a symplectic vector space and global symplectomorphisms". *Math. Z.* 223.4 (1996), pp. 547–559. DOI: 10.1007/PL00004278.

[CS10] Yuri Chekanov and Felix Schlenk. "Notes on monotone Lagrangian twist tori". *Electron. Res. Announc. Math. Sci.* 17 (2010), pp. 104–121. DOI: 10.3934/era.2010.17.104.

[CV21] Man-Wai Mandy Cheung and Renato Vianna. "Algebraic and symplectic viewpoint on compactifications of two-dimensional cluster varieties of finite type". *2019–20 MATRIX annals*. Cham: Springer, 2021, pp. 567–602. DOI: 10.1007/978-3-030-62497-2_35.

[CV22] Roger Casals and Renato Vianna. "Full ellipsoid embeddings and toric mutations". *Sel. Math., New Ser.* 28.3 (2022). Id/No 61, p. 62. DOI: 10.1007/s00029-022-00765-3.

[Dui80] Johannes Jisse Duistermaat. "On global action-angle coordinates". *Commun. Pure Appl. Math.* 33 (1980), pp. 687–706. DOI: 10.1002/cpa.3160330602.

[ES18] Jonathan David Evans and Ivan Smith. "Markov numbers and Lagrangian cell complexes in the complex projective plane". *Geom. Topol.* 22.2 (2018), pp. 1143–1180. DOI: 10.2140/gt.2018.22.1143.

[Eva23] Jonny Evans. *Lectures on Lagrangian torus fibrations*. Vol. 105. Lond. Math. Soc. Stud. Texts. Cambridge: Cambridge University Press, 2023. DOI: 10.1017/9781009372671.

[KK17] Yael Karshon and Liat Kessler. "Distinguishing symplectic blowups of the complex projective plane". *J. Symplectic Geom.* 15.4 (2017), pp. 1089–1128. DOI: 10.4310/JSG.2017.v15.n4.a5.

[KS06] Maxim Kontsevich and Yan Soibelman. "Affine structures and non-Archimedean analytic spaces". *The unity of mathematics. In honor of the ninetieth birthday of I. M. Gelfand. Papers from the conference held in Cambridge, MA, USA, August 31–September 4, 2003.* Boston, MA: Birkhäuser, 2006, pp. 321–385.

[LLW22] Jun Li, Tian-Jun Li, and Weiwei Wu. *Symplectic Torelli groups of rational surfaces*. Preprint, arXiv:2212.01873. 2022.

[LS10] Naichung Conan Leung and Margaret Symington. "Almost toric symplectic four-manifolds". *J. Symplectic Geom.* 8.2 (2010), pp. 143–187. DOI: 10.4310/JSG.2010.v8.n2.a2.

[Mag24] Nicki Magill. "Unobstructed embeddings in Hirzebruch surfaces". *J. Symplectic Geom.* 22.1 (2024), pp. 109–152. DOI: 10.4310/JSG.2024.v22.n1.a3.

[McD11] Dusa McDuff. "Displacing Lagrangian toric fibers via probes". *Low-dimensional and symplectic topology. Proceedings of the Georgia international topology conference, Athens, GA, USA, May 18–29, 2009.* Providence, RI: American Mathematical Society (AMS), 2011, pp. 131–160.

[MS23] Grigory Mikhalkin and Mikhail Shkolnikov. "Wave fronts and caustics in the tropical plane". *Proceedings of 28th Gökova Geometry-Topology Conference (2023)*. International Press, 2023, pp. 11–48.

[MS24] Dusa McDuff and Kyler Siegel. *Singular algebraic curves and infinite symplectic staircases*. Preprint, arXiv:2404.14702. 2024.

[Ono08] Kaoru Ono. "A question analogous to the flux conjecture concerning Lagrangian submanifolds". *Proceedings of the 14th Gökova geometry-topology conference, Gökova, Turkey, May 28–June 2, 2007.* Cambridge, MA: International Press, 2008, pp. 1–14.

[PS24] Leonid Polterovich and Felix Schlenk. "Lagrangian knots and unknots – an essay". *Celebratio Mathematica* Eliashberg (2024).

[San03] Vũ Ngoc San. "On semi-global invariants for focus-focus singularities". *Topology* 42.2 (2003), pp. 365–380. DOI: 10.1016/S0040-9383(01)00026-X.

[Sch24] Joel Schmitz. *A counterexample to Lagrangian Poincaré recurrence in dimension four*. Preprint, arXiv:2410.24102. To appear in Compositio Mathematica. 2024.

[STV24] Egor Shelukhin, Dmitry Tonkonog, and Renato Vianna. "Geometry of symplectic flux and Lagrangian torus fibrations". *J. Topol.* 17.4 (2024). Id/No e70002, p. 56. DOI: 10.1112/topo.70002.

[STW16] Vivek Shende, David Treumann, and Harold Williams. *On the combinatorics of exact Lagrangian surfaces*. Preprint, arXiv:1603.07449. 2016.

[Sym03] Margaret Symington. "Four dimensions from two in symplectic topology". *Topology and geometry of manifolds. Proceedings of the 2001 Georgia topology conference, University of Georgia, Athens, GA, USA, May 21–June 2, 2001*. Providence, RI: American Mathematical Society (AMS), 2003, pp. 153–208.

[UZ25] Giancarlo Urzúa and Juan Pablo Zúñiga. *Wahl singularities in degenerations of del Pezzo surfaces*. Preprint, arXiv:2504.19929. 2025.

[Via16] Renato Vianna. "Infinitely many exotic monotone Lagrangian tori in $\mathbb{CP}^2$". *J. Topol.* 9.2 (2016), pp. 535–551. DOI: 10.1112/jtopol/jtw002.

[Via17] Renato Vianna. "Infinitely many monotone Lagrangian tori in del Pezzo surfaces". *Sel. Math., New Ser.* 23.3 (2017), pp. 1955–1996. DOI: 10.1007/s00029-017-0312-z.

[Yau13] Mei-Lin Yau. *Surgery and Invariants of Lagrangian Surfaces*. Preprint, arXiv:1306.5304. 2013.

[Zun03] Nguyen Tien Zung. "Symplectic topology of integrable Hamiltonian systems. II: Topological classification". *Compos. Math.* 138.2 (2003), pp. 125–156. DOI: 10.1023/A:1026133814607.

[Zun97] Nguyen Tien Zung. "A note on focus-focus singularities". *Differ. Geom. Appl.* 7.2 (1997), pp. 123–130. DOI: 10.1016/S0926-2245(96)00042-3.